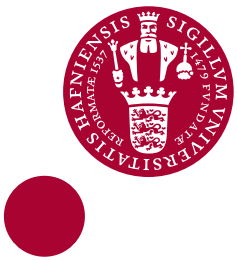

Distances to nearby molecular clouds and star forming regions III. Localizing extinction jumps with a Hipparcos calibration of 2mass photometry

Knude, Jens Kirkeskov

Published in:
arXiv.org: Physics

Publication date:
2010

Document version
Publisher's PDF, also known as Version of record

Distances to nearby molecular clouds and star forming regions III. Localizing extinction jumps with a Hipparcos calibration of 2mass photometry

J. Knude
Niels Bohr Institute, Copenhagen University
Juliane Maries Vej 30, DK-2100 Copenhagen Ø
indus@nbi.ku.dk

June 17, 2010

1 Abstract

We want to estimate the distance to molecular clouds in the solar vicinity in a statistically precise way. Clouds are recognized as extinction discontinuities. The extinction is estimated from the $(H-K)$ *vs.* $(J-H)$ diagram and distances from a $(J-K)_0$ *vs.* M_J relation based on Hipparcos. The stellar sample of relevance for the cloud distance is confined by the FWHM of the $A_V/D_\star(pc)$ or of its derivative. The cloud distance is estimated from fitting a function to the $(A_V, 1/\pi_{JHK})$ pairs in this sample with a function like $arctanh^p(D_\star/D_{cloud})$ where the power p and D_{cloud} both are estimated. The fit follows the $(A_V, 1/\pi_{JHK})_{cloud}$ data rather well. Formal standard deviations less than a few times 10 pc seem obtainable implying that cloud distances are estimated on the $\lesssim$10% level. Such a precision allows estimates of the depths of cloud complexes in some cases. As examples of our results we present distances for ∼25 molecular clouds in Table 2.
Keywords: interstellar medium: molecular cloud distances

2 Introduction

Distances to nearby molecular clouds are essential in many contexts. The more precisely measured ones are often based on dedicated medium band optical photometry of selected stellar types in lines of sight in the general direction of the cloud and its immediate surroundings. It is an advantage that the optical bands are so sensitive to extinction but the same sensitivity of course sets limits on the amount of extinction that may be penetrated.

All photometric systems are not equally suited for extinction purposes since a density of sight lines as high as possible is required to decrease selection effects and all systems are not equally useful for classifying all stellar types. The Vilnius system seems a good choice for optical work because it permits accurate estimates of intrinsic properties such as absolute magnitude and colors for almost any kind of star. The Strömgren-H$_\beta$ system may also be used but for a substantially narrower range of spectral types and mainly for main sequence stars. But it has the great advantage of being based on the extinction free β-index.

After the Hipparcos parallaxes, Perryman et al. ([1997]), have become available combinations with classifications from other sources have been used and resulting in distance − extinctions pairs that estimate the distance to the less obscure parts of molecular clouds, Knude and Høg (1998), Lombardi, Alves and Lada ([2006]).

Alternatively the parallax data already available may be complemented with new observations sensitive to the extinction, e.g. polarization as used by Alves and Franco ([2006], [2007]) in investigations of Lupus clouds and of the Pipe Nebula respectively. Polarization has the advantage that it may be estimated without any knowledge of the target classification and is much more precisely measured than photometry.

A limiting condition of the Hipparcos parallaxes is that they pertain to fairly bright stars measured in the optical and consequently are confined to the low extinction parts of the clouds and only may be used for clouds in the immediate solar vicinity.

If a distance estimate to a cloud is requested photometry is required for a substantial number of stars. Such observations may be rather time consuming despite the advantages brought about by CCD photometry. It would therefore be convenient if a method exploiting available all sky photometric data might be established. It only requires that the photometry may be dereddened and that the dereddened colors may be calibrated in terms of absolute magnitude.

Near infrared data may not be the obvious choice for extinction estimates but some sensitivity to reddening is left and one benefits from the much better penetrating power of the NIR data so the association of the data to the molecular cloud is possibly better established than that of the optical data. Infrared data have been widely used to produce the projection of extinction on the sky in the form of impressive maps and less used for distance determination, e.g. Lombardi, Lada and Alves ([2008]).

For each starget, distance and intrinsic colors should result somehow and the combination of many sight lines may provide a statistical estimate of the cloud distance. As we will notice in the following discussion several regions known to contain molecular material do show an extinction discontinuity at some not very precise distance. The cloud distance may be estimated by the eye but we have investigated some quantitative statistical methods from which the distance intuitively may be estimated – but these methods do not always work in a satisfactory way. Even by limiting the study to the most accurate data, we can not be sure that the data are statistically significant and statistics as the mean, median, standard deviation, σ_{A_V}/A_V versus distance may have shortcomings so they do not immediately guarantee a representative observation of the dust distribution and in particular they do not provide an estimate of the uncertainty of the suggested distance. To meet the required error assessment we suggest instead that some analytical function is fitted to the data defining the extinction jump and that the error may be estimated by the standard deviation from the distance fit. We propose that the sample pertinent for a distance derivation may be extracted from the variation of the line of sight density in a consequential manner. If all stars used to define the jump really are located at a well defined distance, the uncertainty of the estimated cloud distance is on the ±10% level or better. Due to selection effects, some of which are introduced by limiting the JHK photometry to $\sigma_{JHK} \leq 0.040$ or $\sigma_{JHK} \leq 0.080$, originating in the way the sample used for fitting the variation of extinction with distance is defined, the distance estimate may not be robust. But we think that the way we extract this sample – from the variation of the average line of sight density with distance – may be a good approximation to a robust method. At least it is systematic and not based on any personal judgement. Biases are introduced by the co-incidence of the main sequence and giant relations in part of the $(H-K)_0-(J-H)_0$a diagram. The absence of some stellar classes, e.g. ∼G6 – M0, with a certain range of absolute magnitudes, causes the rise of extinction with distance to be more shallow than expected when a molecular cloud is encountered. This have consequences for the statistics and for the estimated cloud distance but we suggest a way to include these stars after the variation of extinction with distance has been computed from the stars earlier than ∼G6 and later than ∼M4.

The paper falls into four parts: In Section 3 we consider ways and means to estimate $D_{cloud} \pm \sigma_{D_{cloud}}$. We present a discussion of about 25 cloud distances in Section 4 and the resulting distances are summarized in Section 5, Table 2.

We have banished the gory details of the main sequence calibration to Appendix A. The discussion of which 2mass stars that may be used for estimating A_J and M_J is deferred to Appendix B.

3 How to estimate the cloud distance? Serpens region as a template

In the following we consider various ways a cloud distance may be estimated and present a procedure we suggest to use with the calibrated 2mass photometry. For details pls. refer to Appendix B.

3.1 Cloud distance estimate from A_V(mean), A_V(median), σ_{A_V} vs. distance

We confine the sample by the photometric precision, quality as well as multiplicity flags and start by including lines of sight outside the frayed cloud confinement. The sample with counts less than the average count, 100/reseau by definition, minus one σ_{count} may indicate cloud directions to a better degree but here we show the result independently of the reseau counts. Including all lines of sight is normally not justified but in the case of Serpens A and B where the preselected solid angles match the clouds well it seems acceptable, see Fig. 36 displaying the distribution of counts. The resulting distances and extinctions are in Fig. 38, 39 indicating a steep rise to $A_V \approx 2.5$ at distances between 160 and 200 pc.

Only 2mass data better than $\sigma_{JHK} < 0.040$ has been used. The eye will probably estimate the cloud distance to be somewhere between 150 and 200 pc. Straižys et al. ([1996]) measure a distance 260±10 pc to this region. The diagram, Fig. 39, shows a few auxiliary curves. The two dashed curves indicate the maximum measurable extinction for the values 11.0 and 14.6 for $V - M_V + 5$ that may be traced by a M4V and a M0V star respectively in a sample with J_{lim} = 14.5 mag. We see that the late M4 – T dwarfs are well confined by such a maximum extinction curve. We also note that the group have a well defined minimum extinction in the distance range from 200 to 400 pc at which distance the minimum extinction starts rising. The extinction discontinuity is well defined by the data. The early and late groups suggest that extinctions between ≈0 and ≈2.5 mag are present in the distance range from ≈60 to ≈400 pc. Within this box the potential K dwarfs are extracted and the Figure shows that these K dwarf candidates support the presence and location of the extinction discontinuity. The median and mean the extinction are shown, computed for 20 pc bins and in 10 pc steps. Beyond about 400 pc the two values stay identical. $\sigma_{A_V}/\sqrt{N-1}$ where σ_{A_V} is the standard deviation and N the number of stars in the distance bin is also indicated. σ_{A_V} is computed in the same intervals as the mean and median. For this field the error of the mean seems to follow the rise of the median extinction. One might think of using some combination of σ_{A_V} and A_V vs. distance to signify the onset of molecular extinction (Padoan, Nordlund, Jones ([1997]) and the Lada et al. ([1994]) σ_{A_V} vs. A_V variation). Between 600 and 1200 pc the median has a constant slope implying a constant dust density beyond the Serpens Cloud and with a known gas/dust ratio the average line of sight number density of hydrogen may be determined. See the discussion in the next Section on how the variation of the line of sight mean density may be used to locate the cloud.

The Serpens 2by2 region may be particularly well behaved since the both the mean and median A_V starts rising at 200 pc as do $\sigma_{A_V}/\sqrt{N-1}$. It is, however, difficult to quantify the cloud distance and its uncertainty from e.g. the median extinction's variation. An average of the distances where the median starts and stops rising could possibly be used as the distance and half their difference as an indication of the uncertainty. As Fig. 39 indicates the distance to the cloud is based on all three groups of stars implying that the relative error on the individual stellar distances formally range from ≈10% to ≈40% with an overweight of the smaller ones.

3.2 Distance indications from other statistics

When approaching a molecular cloud the interstellar density will jump up when the cloud is penetrated. When the density increase is large enough over a short distance the increase is reflected in a rise in A_V despite A_V is the integrated of the density along the line of sight. In order to cause a discontinuity the cloud extinction, sampled over a short distance, must be comparable to or exceed the extinction accumulated along the line of sight to the cloud. With enough data to form derivatives we would expect the derivative $\partial n_H/\partial D$ where n_H cm^{-3} is the average number density of atomic hydrogen and D the distance to show a dramatic increase over a short distance range. n_H cm^{-3} is formed by converting A_V to N_H with the canonical gas to dust ratio. Fig. 1(a) shows the variation of the line of sight density of neutral hydrogen for the Serpens 2by2 region and a very sharp increase is noticed at ∼200 pc. The asymptotic value of n_H is ≈1 atom/cm^{-3} fairly close the the mean density of the diffuse interstellar medium in the solar vicinity. The constant part of the tail results when the clouds contribution to the average line of sight density becomes negligibel compared to the contribution from the intercloud diffuse medium: $N_H(cloud)/D < n_H(intercloud)$. Identical to the distance range where the slope of $A_V(median)$ becomes vitually constant. The (b) part of the same figure is the derivative of the density with respect to distance (in cm) and again we notice a change at ∼200 pc. Part (c) of Fig. 1 is a zoom of the (b) frame

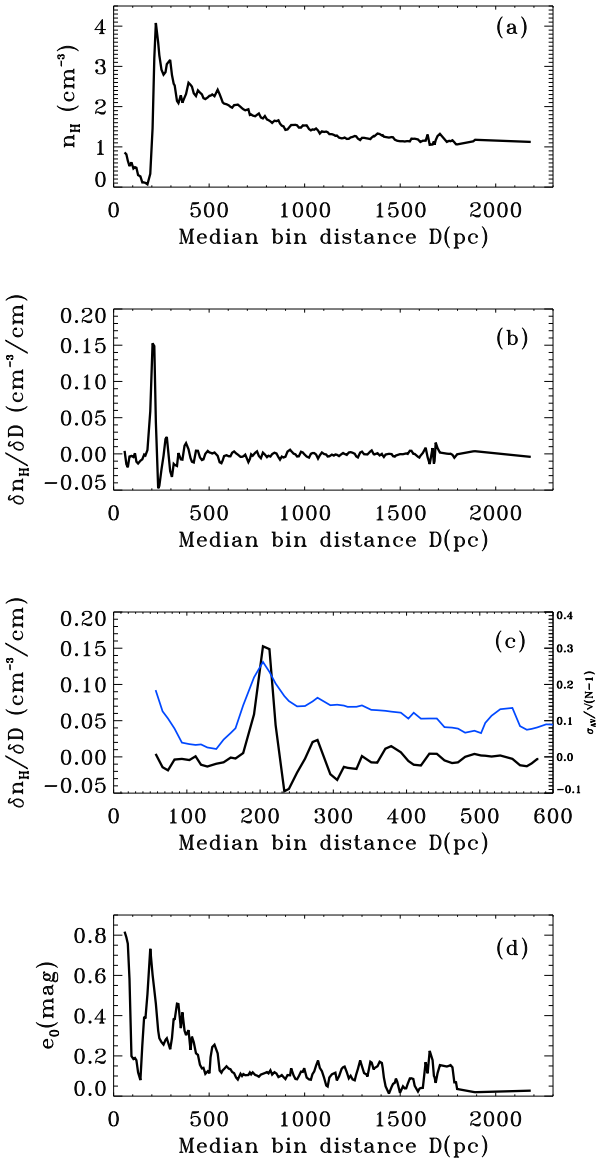

Figure 1: Statistics for the Serpens 2by2 region. **(a)** Mean line of sight density n_H cm^{-3}. **(b)** The derivative of the mean density. **(c)** Zoom of **(b)** and $\sigma_{A_V}/\sqrt{N-1}$ is plotted as the upper curve and is to the right hand scale. **(d)** Mean V-extinction, e_0 in a standard cloud

displaying the effect of an increasing density over the distance range from ~180 to ~210 pc. The (c) frame also contains a sort of mean dispersion $\sigma_{A_V}/\sqrt{N-1}$ pertaing to the 20 pc distance bins.

Early studies of the patchy structure of the ISM, assuming that the interstellar medium was constituted by a single (or two) type(s) of interstellar cloud(s) floating in an intercloud medium provided a detailed statistical method to estimate the extinction e_0 in the characteristic cloud, Münch ([1952]). This method requires a data set of distance and extinction pairs, just what we get from the present study. The characteristic cloud extinction is given by the expression $e_0 = M_2/M_1 - M_1(1 + (\Delta D/D)^2/12)$. M_1 is average A_V and M_2 equals the average of A_V^2 in a distance interval ΔD wide and centered on the distance D. Frame (d) of Fig. 1 displays this simple statistics. The e_0 expression is valid when $(\Delta D/D)^2/12)$ is less than unity which is not quite the case for the first distance bins. In these bins σ_{A_V} is large which together with the small average extinctions raises the e_0 estimates. Beyond ~500 pc e_0 becomes constant, settling around A_V=0.1 mag. Converting to a color excess in the *uvbyβ* system the characteristic cloud reddening becomes ≈0.040, the exact value depends on the choice of R_V. The e_0 ≈0.04 is close to the values ranging from 0.025 to 0.045 calculated from *uvbyβ* photometry of F stars within 150 pc, Knude ([1979c]). Measured reddenings of "isolated" clouds were in the range from ~ 0.02 to ~0.11 , Knude ([1979a]). This coincidence is taken as evidence that in a statistical sense our present extinction and distance estimates imply results comparable to those obtained by independent methods.

Frame (d) of Fig. 1 further contains three peaks at 195, 335 and 530 pc respectively which probably may be taken as evidence for the presence of molecular clouds, at least for the 195 and 335 peak's part. That the large e_0 values popping up in a few adjacent distance bins may indicate the distance to a molecular cloud may not be unexpected after all. When $(\Delta D/D)^2/12) << 1$ $e_0 \approx M_2/M_1 - M_1 = \sigma^2_{A_V}/A_V = \sigma_{A_V} \times \sigma_{A_V}/A_V$. And according to Fig. 39 σ_{A_V} as well as σ_{A_V}/A_V have local maxima at ≈200 pc. The 335 pc peak may be an artefact caused by a local minimum in the median A_V and there is no local maxima in σ_{A_V}/A_V at this distance. The σ_{A_V}/A_V minimum is possibly not real since stars at 335 pc with $A_V = 3 - 4$ is not measurable by our method: the missing M0 – M4 dwarfs (see the discussion of Fig. 38).

A well behaved discontinuity as the one in the 2by2 Serpens region offers several options for the distance estimate: mean and median of A_V, σ_{A_V}, the mean dispersion $\sigma_{A_V}/\sqrt{N-1}$, the mean line of sight density n_H, $\partial n_H/\partial D$, e_0 or equivalently $\sigma_{A_V} \times \sigma_{A_V}/A_V$. Of these n_H and $\partial n_H/\partial D$ display sharp peaks at what we interpret as the cloud distance. The mean dispersion of A_V have a broader peak than the derivative of the mean line of sight density. These estimators do not provide an immediate uncertainty on the distance but indicate a distance range in which the cloud is located.

3.3 An algoritm fitting the extinction – distance variation at an extinction jump

Due to the rather few distance – extinction pairs that most often have been available in the direction of a cloud most studies of cloud distances suggest that the cloud distance may be estimated from the distance where the increased extinction is first noticed and the location of this rise is furthermore estimated by the eye. This would of course be correct if the stellar distances were perfect with only negligibel errors. Other studies claim to have a stellar density high enough to identify the backside of the extinction rise as well as the front, Whittet et al. ([1997]) for the Chamaeleon II cloud, and equivalates the cloud distance to the mean of these two distances thus also implying an uncertainty of the distance estimate.

With the 2mass data we may often have an observed stellar density that is higher than otherwise have been the case and we may consider a more quantitative approach.

The A_V vs. stellar distance diagram is characterized by a set of stars in front of the cloud measuring only the extinction of the diffuse interstellar medium until the cloud is reached when the extinction diplays a steep rise over a short distance range.

The extinction rise shall be matched by a function staying ~constant until it displays an almost vertical growth. A horizontal and a vertical line have been used to match thess trends but in particular the vertical part seems difficult to accomodate in a systematic and robust way. A critical issue is how far beyond the rise stars can be included in the distance determination?

A function $arctanh^p(x)$ with $0 \leq x < 1$ simulates a combination of a horizontal and a vertical line rather

well. And yes, there may be other functions serving our purposes. Our choice is not completely arbitary as judged from the standar deviations obtained. Its logarithmic presentation $arctanh(x) = 0.5 \times log_e \frac{1+x}{1-x}$ where x is short for $\frac{stellar\ distance}{cloud\ distance}$ and p is a power introduced to emphasize either the vertical trend or the horizontal one whichever the least square procedure selects. In order to use the logarithmic expression we must introduce a maximum distance beyond which no stars are included in order to keep the parameter $x = D_\star/D_{max}$ less than unity. NOTE: D_{max} is not the cloud distance but defines the sample used to estimate $D_{cloud} < D_{max}$.

A non trivial problem is, however, to define the sample to be included in the fitting procedure. It is a question of how large distances can be included and still be pertinent for the cloud distance. Stars far behind the cloud have the large cloud extinction plus a contribution from the diffuse medium but should not enter the cloud distance determination. As seen in Fig. 39 the jump contains several G6V-M0V stars that have a calibration standard deviation of only $\sigma_{M_J} \approx 0.1$ mag equivalent to a distance uncertainty ≈10%, see Fig. 31. If the Serpens 2by2 cloud is at 200 pc we should include stars in the interval from 180 to 220 pc. In order to exclude less reddened stars probably beyond the cloud distance and not including distant stars showing the extinctions in the jump but not assisting assessing the cloud distance we make a selection for the fit. For the selection we use a curve A_V *vs.* $arctanh^p(\frac{D_\star}{D_{max}})$ to set an upper distance for each A_V. After some experimenting our choice is p=4 since this value emphasize the shallow part of the data. Note that p=4 is only used for selecting the cloud sample when the cloud distance is derived from the curve fitting p$\pm\sigma_p$ also results. From the density variation in the Serpens region D_{max} becomes 250. The 250 pc is not a general upper limit for stars included in the curve fitting: In Fig. 2 we notice that the requirement $A_V(\star) > arctanh^4(\frac{D_\star}{D_{max=250}})$ excludes several stars $D_* \lesssim 200$ pc with a low extinction.

A systematic definition of the fitting sample is required and should be independent of any personal judgement. D_{max} is determined from the variation of the line of sight average density n_H or its derivative *vs.* distance and is formally defined as the maximum of the FWHM points. For Serpens ~250 pc is the largest of the FWHM distances. We confine the fitting sample to the stars that are closer and more extincted than indicated by the curve $A_V(sample\ confinement) = arctanh^4(\frac{D_\star}{D_{FWHM,max}=250})$.

A procedure proposed to estimate the cloud distance:

• *confine the cloud on the sky: contours from star counts or the average of the* $(H-K)$ *color formed in reseaus.* $\overline{H-K}_{res}$ *is preferred to star counts since it appears to be more directly linked to the extinction. The reseau is dynamically defined to have a radius implying 100 stars/reseau on the average. The minimum cloud* $\overline{H-K}_{res}$ *is estimated from* $\overline{H-K}_{res}$ *vs. position diagrams as the ≈maximum of the almost constant value of* $\overline{H-K}_{res}$ *outside the cloud. Fig. 7 is an example where* $\overline{H-K}_{res}$ *= 0.23 is evident as the maximum for lines of sight b ≲ -12°. All lines of sight with a reseau average exceeding this ≈maximum are accepted as pertaining to the cloud.*

• *run codes on the contour sample extracting stars from the* $H-K$ *vs.* $J-H$ *diagram:* $O-G6$ *(primary),* $M4-T$ *(secondary),* $G6-M0$ *(tertiary) to estimate* $(J-H)_0$ *and* M_J *and compute the* $(D_\star, A_V(\star))$ *pairs.*

• *bin distance range and use* $(D_\star, A_V(\star))$ *to compute* $(D_\star(median), \overline{n}_H(los, median))$

• *see if* $\overline{n}_H(los, median)$ *or* $\delta\overline{n}_H/\delta D_\star(median)$ *displays a peak. Use* $D_{FWHM,max}$ *of the* $\overline{n}_H$ *or* $\delta\overline{n}_H/\delta D_\star(median)$ *variation with distance to confine the sample to be used for the curve fitting:* $A_V(\star) > arctanh^4(\frac{D_\star}{D_{FWHM,max}})$. *Note: in the selection p=4.*

$\overline{n}_H$ *is proportional to* $A_V(\star)/D_\star$. $\overline{n}_H$ *is computed from the median* A_V *in distance bins but if the density of data points is not sufficient for the* $\overline{n}_H$ *vs.* D_{median} *variation is replaced by the distribution of individual values* $(A_V/D)_\star$ *from which ~* $D_{FWHM,max}$ *is estimated.*

• *fit* $A_V(jump) = arctanh^p(\frac{D_\star}{D_{cloud}})$ *to this sample.* $D_{cloud} \pm \sigma_{D_{cloud}}$ *and* $p \pm \sigma_p$*is returned. The procedure used for fitting* D_{cloud} *and* p *is an implementation of the nonlinear Marquardt-Levenberg algoritm. The algorithm varies the parameters* D_{cloud} *and* p *in search of the minimum in the sum of the squared residuals. The iteration stops when convergence is attained.*

• *the contour* $\overline{H-K}_{res,\ CLOUD}$ *defining the cloud perimeter and* D_{max} *are the two most critical parameters and must be estimated with care*

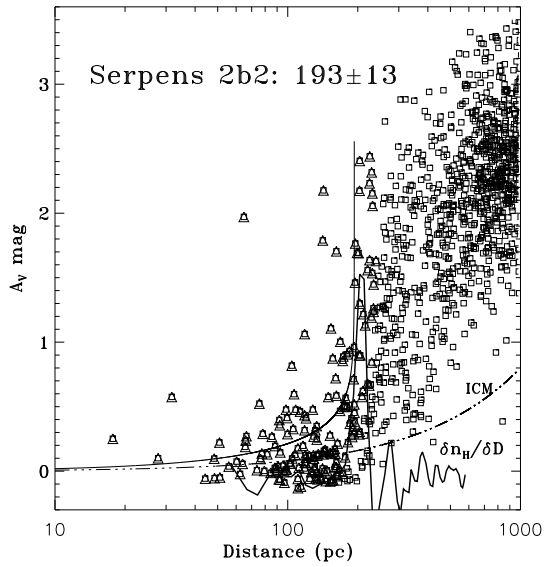

Figure 2: The Serpens 2by2 region with the fitted $arctanh^p(\frac{D_\star}{D_{cld}})$ function shown as the solid curve. The sample used for the fit is overplotted with triangles. For reference a scaled version of $\partial n_H/\partial D$ is shown. The dash – dot curve illustrates a previous estimate of the intercloud density, Knude ([1979b]). The Serpens 2by2 template data are also treated in App. B Fig. 39

As a template we use the Serpens data. The derivative's, $\partial n_H/\partial D$, variation with distance implies D_{max}=250 pc. The sample are stars above the curve $A_V = arctanh^4(\frac{D_\star}{250})$. The fitting sample is shown in Fig. 2 as the combined squares/triangles. Then the fitting procedure is run. The convergence normally takes place after $\lesssim$10 iterations. For the Serpens 2by2 area the final distance becomes D_{cloud}=193±13 pc. The resulting fit is shown in Fig. 2 together with $\partial n_H/\partial D$, there is a good coincidence between the resulting cloud distance and the location of the ($\partial n_H/\partial D$) peak: the ($\partial n_H/\partial D$) peak may be used to indicate the approximate cloud location and not least provides the distance range in which the cloud is situated.

4 Examples of cloud distances

Considering the multitude of local interstellar clouds we have to be selective and only consider a few examples, ~25, of cloud distance determination from the *JHK* 2mass data. Most interesting among the local clouds are the star forming molecular clouds since many of the parameters needed for understanding the importance of the environment for the onset of the star formation depend on some power of the distance. The distance is of course also an important issue when model parameters e.g. from evolutionary models of proto and PMS stars are to be compared with observational data.

During the work with the proposed method a new opportunity for checking the suggested distances has become available with the advent of the VLBI/VLA astrometric observations of PMS stars and masers resulting in unprecedented parallaxes to targets probably associated to star forming clouds.

4.1 The Taurus star forming region

The region covers a substantial part of the sky with longitude ranging from ~154° to ~180° and latitude from -24 to the galactic plane. We have distributed 16 2×2 □° regions cowering the main features of the cloud as indicated by CO intensity maps and compiled 2mass data with σ_{JHK} better than 0.080 mag. Taurus is of special interest since its distance has been measured to 137 pc using VLBA astrometry resulting in ~one percentage accuracy which is an order of magnitude better than what has been obtained previously, Torres et al. ([2007]).

The VLBA astrometry tracking the path on the sky resulting from the yearly and proper motion of naked T Tauri stars in the cloud provides individual distances with a precision better than 1 pc. Furthermore such a precision allows the depth of the cloud to be no less than about 20 pc. A mean distance of 137 pc corroborates the 139±10 pc deduced from approximate parallaxes based on proper motions, Bertout and Genova ([2006]).

Confining the sample by the photometric precision alone may include lines of sight outside the frayed cloud confinement. The sample with counts less than the average count, 100/reseau by definition, minus one σ_{count} may indicate proper cloud directions to a better degree. The outcome is shown in the middle panel of Fig. 3 indicating a steep rise to A_V ≈1.5 at distances between 100 and 120 pc. Extinctions exceeding 2 mag are noticed for the same distance range. Another steep rise is noticed at ≈170 pc increasing A_V from ~1.5 to ~3.0. We can not decide whether this dual structure is due to the distribution in depth of the Taurus complex or is an effect of the incompleteness of the tracing sample causing the sloping appearance of the extinction variation with distance as discussed in Fig. 38.

The upper panel of Fig. 3 is the extinction variation from a combination of all data in the 64 square degrees from the 16 2×2 □° areas without considering the cloud containment neither from the reseau counts nor from a lower $\overline{(H-K)}_{reseau}$ limit. A rather well defined peak in the average lines of sight density has an upper FWFM distance at D_{max} ≈ 200 pc. The resulting fitting sample is marked as gray points in the upper panel and from the curve fit a distance D_{Taurus}=127±2 pc is computed. The small dispersion is caused by the large number of stars in the sample. Notice that a substantial number of nearby low extinction stars are not included in the curve fitting. Also notice a number of stars at ≈80 pc with extinction larger than 1 mag. These small distances displaying large extinctions are possibly due to giants mistaken for dwarfs.

In the central panel the sample is constrained to the stars with reseaus with counts less than (<count> - 1×$\sigma_{<count>}$). D_{max} has now increased to ≈300 pc and D_{Taurus}=162±15 pc is computed. The vertical dashed line at 137 pc is the average of the VLBA/VLBI paralaxes and the dispersion ±19 pc is an indication of the depth of the Taurus complex from these precise data.

The lower panel is perhaps the most interesting one since it covers the region where the three low mass YSOs with VLBA/VLBI parallaxes are located. The data are now confined by two criteria: σ_{JHK} ≤0.040 mag and $\overline{(H-K)}_{reseau}$ > 0.20. D_{max} = 250 pc, which comply to the formal definition of D_{max}, implies D_{Taurus} = 147±10 pc. Reducing D_{max} with with 25 and 50 pc changes the D_{Taurus} estimate to 130 and 125 pc respectivly without changing the standard deviation. We suggest 147±10 pc as representative and this distance is furthermore only one sigma separated from the VLBA distance of 137 pc.

The three different ways of selecting the data from which the fitting sample was selected result in three different distance estimates for Taurus: 127±2, 162±15 and 147±10 pc and illustrate the importance of being systematic. The distance resulting from our procedure 147±10 pc is fortunately the one agreeing best to the VLBA/VLBI parallax 137 pc.

4.2 The ρ Ophiuchus star forming region

Similarly we have used the extinction map by Cambrésy ([1999]) for the ρ Ophiuchus complex of clouds to define the solid angle confining the extinction associated with ρ Oph. In this area we have extracted the 2mass data with σ_{JHK} ≤0.080 mag. We may refine this sample by changing the area, error and value of the reseau means. Fig. 4(a) shows the combined area for which data are extracted (dotted outline), The area covering the core region, LDN 1688, and containing the two low mass YSOs, whose positions are marked by crosses, is shown as the dashed confinement. The two squares in the southern extention indicate LDN 1672 (the southern one) and LDN 1675 respectively. According to Cambrésy's map the extinction through the southern feature does not reach the blocking extinction met in the cloud core and may therefor suit our approach better – that is if all the clouds are spatially associated. Fig. 4(b) shows the resulting distance – extinction diagram. After confining the sample to the most precise photometry, σ_{JHK} < 0.040 mag and only using stars in reseaus where the reseau mean exceeds 0.20 mag. The outlines in Fig. 4(a) is defined by stars with $\overline{(H-K)}_{res}$ mean values between 0.20 and 0.24. Fig. 4(b) shows resulting extinctions for stars within 500 pc. The variation of n_H with distance is not well defined, but it does indicate D_{max} ≈230 pc, a value corroborated by the median extinction,

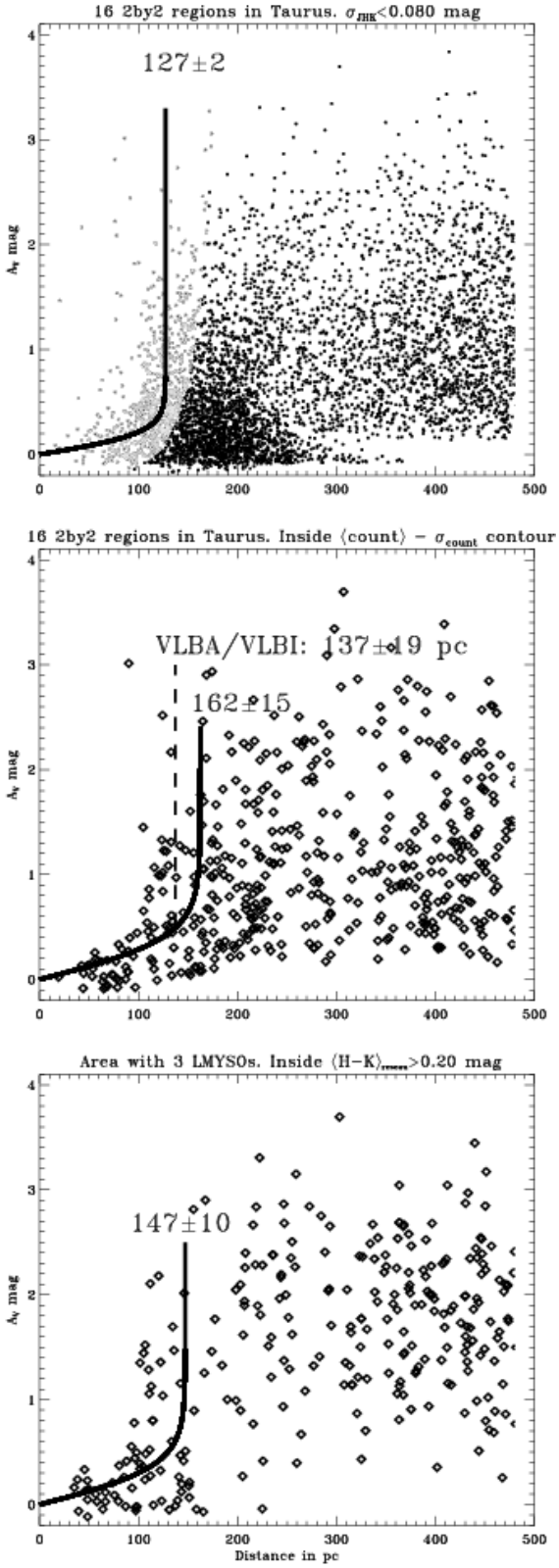

Figure 3: Three different selections of a Taurus sample. The *lower panel* displays the outcome of the method we suggest to use. *Upper panel*: Stellar sample with σ_{JHK} ≤0.080 mag distributed in 16 2×2 □° in Taurus. Cloud fitting sample are the light gray points. *Middle panel*: stars in the 16 2×2 □° in Taurus within the (<count>$_{res}$ - 1×σ_{count}) contour but including σ_{JHK} ≤0.080. *Lower panel*: Region containing the three low mass YSOs HP Tau, Hubble 4, HDE 283572 for which VLBA astrometry has been performed. See Fig. 2 of Loinard et al. ([2008]). The 137±19 pc indicated in the *middle panel* is from Loinard et al. and the ±19 pc is meant to i ndicate the possible depth of the complex of clouds. The *lower panel* data ar for longitude range [167°, 177°] and latitude range [-16.8,-14.8], the region containing the T Tau stars with VLBA/VLI parallaxes. Only stars with σ_{JHK} ≤0.040 mag and located in reseaus with $\overline{H-K}_{reseau}$ > 0.20. With D_{max} = 250 pc the resulting fit is D_{Taurus} = 147±10 pc which we propose for the Taurus distance

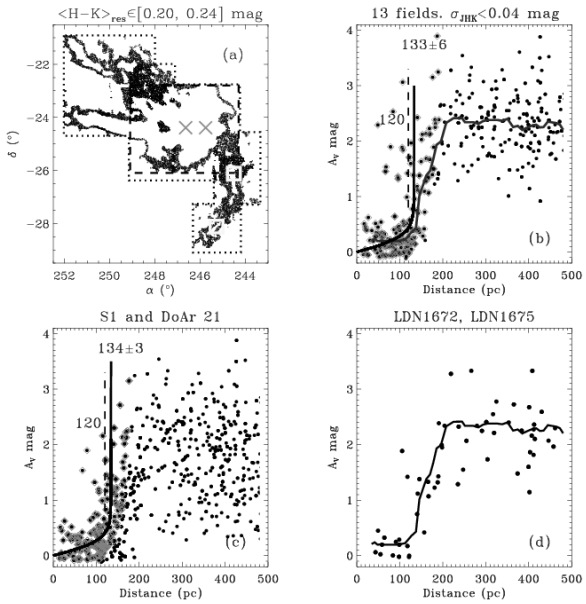

Figure 4: Ophiuchus. (a) Dotted boxes are the total area searched in 2mass. The perimeter is made up by the stars with $\sigma_{JHK} < 0.080$ mag and $\overline{H-K_{res}} \in [\ 0.20, 0.24]$. The central dashed box confines the ∼1.5 □° covering L1688, the dense core of the ρ Oph complex and contains Oph S1 and DoAr 21 marked by the two crosses. (b) Extinction - distance pairs for stars in reseaus with $\overline{H-K_{res}} > 0.20$ mag and with $\sigma_{JHK} < 0.040$ mag. The solid curve indicates the variation of the median extinction. The sample used for the curve fitting is inscribed in diamonds. We note that the fitted distance corresponds to the distance where the median extinction starts rising. (c) Same as for panel (b) but without any restrictions on $\overline{H-K_{res}}$. The dashed line at 120 pc indicates the lower limit of the range 120 – 150 pc suggested by Knude and Høg ([1998]). (d) Extinction vs. distance for the two south eastern boxes covering the Arc. Mainly the clouds L1675 and L1672 (upper and lower square in (a) respectively)

also shown in Fig. 4(b), that stays constant immediately behind the cloud. The constancy of the median sets in at about the same distance ≈230 pc. Stars used for the distance estimate are inscribed in diamond symbols. The estimated distance for the stars inside the $\overline{H-K_{res}} = 0.20$ mag contour becomes $D_{\rho\ Oph} = 133\pm6$ pc. The distance to the core region is shown in Fig. 4(c) and here we did not apply a $\overline{H-K_{res}}$ criterion – not needed anyway because any reseau does have a high mean $(H-K)$ value. The distance estimate does not change $D_{LDN\ 1688} = 134\pm3$ pc. Finally Fig. 4(d) shows the extinction jump in the southern extension, often called the arc, and both the $\overline{H-K_{res}} > 0.20$ and the $\sigma_{JHK} < 0.040$ mag criterion are applied. The solid curve is the median for the complete cloud complex and the distance of LDN 1672 and LDN 1675 is compatible with ∼133 pc. We propose accordingly that the distance to the ρ Oph star forming complex is 133±6 pc not accounting for the depth of the complex.

With the advent of VLBA astrometry of low/median mass YSOs to a precision of a mere few percent the derivation of distances to nearby star forming clouds seems to have entered a new era. Loinard et al. ([2008]) measured parallaxes for the two such systems, S1 and DoAr21, in LDN 1688 and found a resulting distance they refer to as the cloud distance: $120^{+4.5}_{-4.2}$ pc. A similar distance, 119±6 pc, was suggested by Lombardi, Lada and Alves ([2008]) from a maximum likelyhood study of a preselected sample. In a study of the distribution and motion of the gas in the ρ Ophiuchi cloud from high resolution spectroscopy of Hipparcos stars Snow, Destree and Welty ([2008]) find a most likely distance to the dense molecular cloud 122±8 pc and that the more diffuse component is distributed between ∼110 and ∼150 pc. Knude and Høg ([1998]) proposed ∼120 pc as the distance to the Ophiuchus region and suggested 150 pc as an upper limit to the complex of clouds.

4.3 The LDN 204 and LDN 1228 filaments

These two filaments host four isolated cloud cores, Chapman and Mundy ([2009]). Examples of cores with no YSOs (LDN 204) and with 7 YSO candidates (LDN 1228). The two filaments are rather nearby 125±25 and 200±50 pc as quoted by Chapman and Mundy and may thus be within reach of the *JHK*-photometry. Since there are three different YSO classes in LDN 1228, Class II and earlier, a more precise distance estimate could be useful for calibrations of PMS models.

4.3.1 The LDN 204 filament

The LDN 204 filament is an interesting feature because it is nearby and is silhoutted against the extended HII region powered by ζ *Oph* at a distance of only 140 pc and $\approx 3^\circ$ away from LDN 204. The filament displays a most regular polarization pattern and is thus a good candidate cloud for studying the influence of the magnetic field on possible star formation. Part of the filament is included in an extention of the c2d study of molecular cloud cores as a specimen of the cores presently not actively forming stars, Chapman and Mundy ([2009]). We might have included this cloud under the ρ *Oph* heading since it could be part of the Ophiuchus complex of clouds as indicated by the extinction map in Lombardi et al. ([2008]) and it bears a certain similarity to the appearance of Lupus I, Fig. 9.

The cloud outline and the extinction vs. distance may be seen in Fig. 5. Several other clouds than LDN 204 appear in panel (a). We have assumed them to be spatially associated.

The resulting distance is found as 133±6 pc identical to the distance suggested for the central clouds in the Ophiuchus complex. So from the distance point of view LDN 204 and its nearest string of cloud companions seem to belong to the Ophiuchus group of clouds.

4.3.2 The LDN 1228 filament

Chapman and Mundy ([2009]) cite a distance 200±50 pc for this filament. Conelly, Reipurth and Tokunaga ([2008]) prefer a distance 175 pc from the compilation of LDN distances by Hilton and Lahulla ([1995]) formed as an average of two literature values 150, 200 pc. The filament is known to contain HH objects within its confinement. We have taken the nominal position (l, b) = (111.66, +20.22) and extracted the 2mass stars within a 4×4 $\square^\circ$ area for further study. Figure 6 (a) displays stars with $\sigma_{JHK} < 0.060$ mag and $\overline{H-K}_{res} > 0.19$. The HH 199 and HH 200 positions are also shown. Note that the σ_{JHK} criterion has been relaxed somewhat to have enough stars for the distance estimate.

After applying the arctanh fit on the stars with D_{max} = 400 pc the LDN 1228 distance is estimated to 235±23 pc. The precion is inferior to the one for the LDN 204 distance but is none the less on the $\lesssim$10% level.

Chapman and Mundy ([2009]) present model parameters for their YSO candidates. If a change of distance from 200 to 235 pc applies luminosities go up by ≈40%. NOTE that Chapman and Mundy ([2009]) also suggest a variation of the MIR extinction law; most pronounced in the possible outflow regions but we have used our standard law despite this fact. This may be justified by the relative shallowness of the 2mass data not probing all the way to the PMS stars.

4.4 LDN 1622 and 1634 near Orion

The Orion giant complex requires a study by itself and is not included in the present work. We just report our results for directions towards the two isolated cometary clouds LDN 1622, (l, b) = (204.7°, -11.8°), and LDN 1634, (l, b) = (207.6°, -23.0°) both actively forming stars and possibly associated to the Orion complex.

4.4.1 LDN 1622, 1621,1617, and 1624

We have previously reported a distance estimate based on calibrated Tycho-2 photometry and Michigan classification, Knude et al. ([2002]). In this region there is an indication that the first dust is met somewhere between 160 and 200 pc. The use of the combination of Hipparcos and Michigan classification, Fig. 6 – 7 of Knude

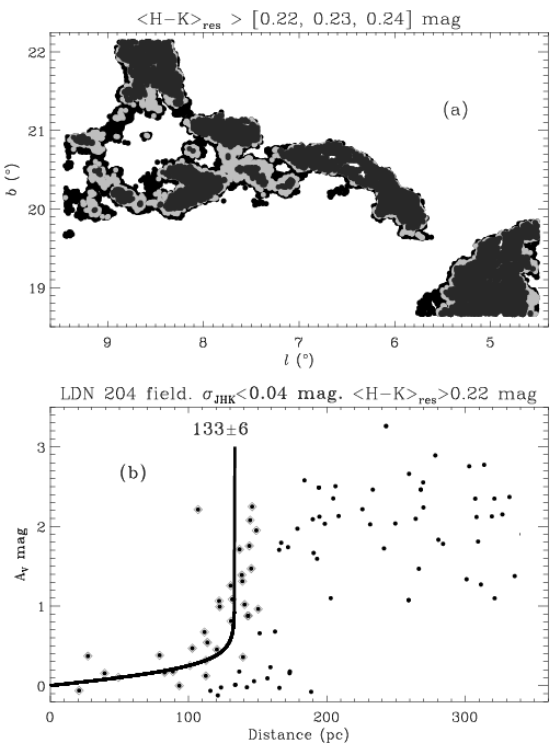

Figure 5: LDN 204, which does not host star formation. (a) Stars with σ_{JHK} ≤0.080 mag and $\overline{H-K_{res}}$ greater than 0.22, 0.23 and 0.24 respectively. LDN 204 is the curved feature at the diagrams center. (b) Extinction - distance pairs for stars in reseaus with $\overline{H-K_{res}} > 0.22$ mag and with $\sigma_{JHK} < 0.040$ mag. The solid curve indicates the arctanh fit to the sample confined by D_{max} = 250 pc and $D_{LDN\ 204}$ = 133±5 pc

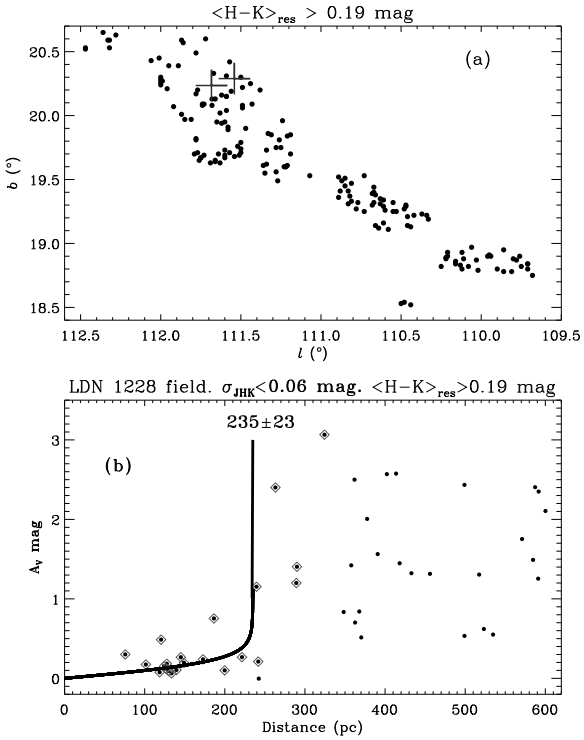

Figure 6: LDN 1228. (a) Collection of stars with σ_{JHK} ≤0.060 mag and $\overline{H-K_{res}}$ greater than 0.19. The lower left plus sign indicates the location of HH 200 IRS and the upper right is HH 199 both of which happens to be located at the nominal center of LDN 1228. (b) Extinction - distance pairs for stars in reseaus with $\overline{H-K_{res}}$ > 0.19 mag and with σ_{JHK} < 0.060 mag. The solid curve indicates the arctanh fit to the sample confined by D_{max} = 400 pc. $D_{LDN\ 1228}$ = 235±23 pc

et al. ([2002]), presents a complex picture of the distribution of extinction with distance: we see extinction discontinuities at approximately 160, 250 and 400 pc depending on the angular separation from the center of LDN 1622. Due to the spatial incompleteness of the parallax catalog these distances, apart from the smallest one, may be due to selection effect. The latter, however, comply with the canonically accepted Orion complex distance.

We have extracted 2mass data from a ≈20□° area with σ_{JHK} ≤0.080. We have chosen $\overline{H-K}_{res} \geq 0.23$ to represent a sight line with extinction relevant for LDN 1622. This choice is corroborated by panel (b) of Fig. 7 where we have plotted $\overline{H-K}_{res}$ vs. latititude. Below -12° $\overline{H-K}_{res}$ is fairly constant and stays below ≈0.23 mag which accordingly is taken to represent the maximum value valid for lines of sight outside the clouds. A relative zero level so to say. At -12° the maximum $\overline{H-K}_{res}$ rises dramatically. Panel (b) also displays $\overline{H-K}_{res}$ values found at the nominal latitude of LDN 1622, 1621, 1617 and 1624 in rising order. The declining run of the maximum $\overline{H-K}_{res}$ may indicate that we are moving from the head of a cometary cloud out in its tail. Note, however, that this is *not* the usual orientation of the cometary tail. See Fig. 1 of Reipurth et al. ([2008]) where LDN 1622's tail is ∼perpendicular to the LDN 1622 LDN 1617 connection. Panel (a) shows the distribution on the sky of reseaus with $\overline{H-K}_{res} > 0.23$ mag. We note that LDN 1622, 1621 and 1617 are located along the axis of the cloud.

The cloud sample is constrained by σ_{JHK} ≤0.040 and $\overline{H-K}_{res} > 0.23$. There are too few stars to use the ideal procedure so we are obliged to use the distribution of individual values of $A_V/D_\star$ and we accept D_{max} = 350 from this distribution. The curve fitting returns $D_{LDN\ 1622}$ = 233±28 pc for the 131 stars used in the fit. The number of stars showing the extinction discontinuity is less than 20 as panel (c) shows. These numbers are quite interesting considering that the 2mass extraction we search contains more than 32000 stars. Assuming that the cloud outline in panel (a) is due to a single structure, 233 pc may apparently also apply to LDN 1621, 1624 *and* to LDN 1617. That LDN 1622 and LDN 1617 should be associated is, however, contested by a V_{LSR} difference ≳5 km/s, Reipurth et al. ([2008]).

Panel (c) does show a group of four stars between 170 and 200 pc showing an extinction ≈1 mag perhaps corroborating the 160 – 200 pc estimate from Knude et al. ([2002]). One of the Hipparcos stars, HD 39572, with a measured distance of $199\pm^{55}_{33}$ and classified as B9 is marked with a triangle in panel (a) and (c). Assuming that it is a main sequence star implies A_V ≈0.1 mag. It is in other words not affected by the LDN 1622 extinction. The stars position in panel (a) is inside the cloud demarcation so it may in fact provide a lower distance limit since it is unreddened.

4.4.2 LDN 1634

LDN 1634 may resemple LDN 1622 since it is located outside the Barnard Loop and like LDN 1622 contains a number of young stellar objects. In a study of these YSOs and their outflows Bally et al. ([2009]) have estimated the clouds spatial location and its implications for its distance from the Sun from the influx of radiation required to keep its rim ionized. This ionization distance is in accord with the canonical Orion distance of 400 pc. The mass following from a 400 pc distance implies a star formation efficiency of ∼3% in LDN 1634. Fig. 8 shows the 2mass data used for our discussion. Panel (b) is $\overline{H-K}_{res}$ vs. longitude and support our choice of 0.15 mag as the lower reseau limit for the cloud lines of sight as evident for $l \gtrsim 208°$. The distribution on the sky appears from panel (a) where we also indicate the location of the sample used for the distance fit. Contrary to LDN 1622 LDN 1634 has a very frayed appearence. The line of sight mean extinction, $A_V/D_\star$ mag/pc, has a clear peak but is probably influenced by the presence of matter at distinctly different distances (only three stars in fact). D_{max} = 425 pc is accepted and the fit returns $D_{LDN\ 1634}$ = 266±20 pc. The fitted curve is shown in the (c) panel of Fig. 8. We have also extracted stars with Hipparcos parallaxes from the total area in panel (a) and for those with a Michigan classification we estimate the color excess. The variation of extinction with distance for these stars closer than 450 pc is shown as triangles in panel (c). Two stars at ∼250 pc in fact have an extinction A_V ≈1 mag. So we may possibly maintain that some material displaying extinction exceeding what is expected from the diffuse ISM is found at 250 – 266 pc. A visual inspection of Fig. 8 may even suggest a distance ≈200 pc. This short distance estimates are significantly different from the detailed "ionization" distance ∼400 pc to

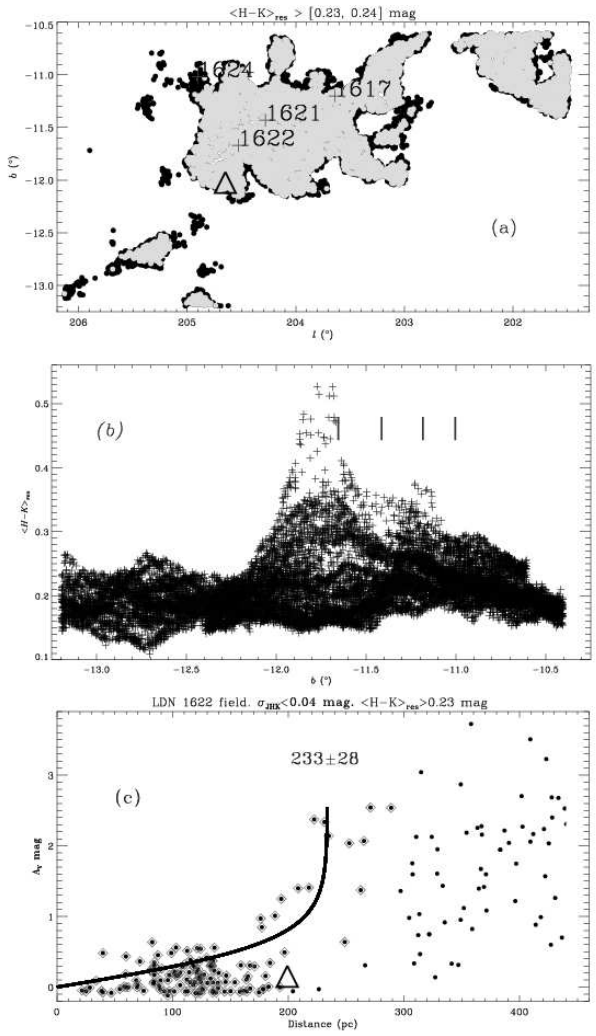

Figure 7: The LDN 1622 area. (a) Collection of stars with σ_{JHK} ≤0.040 mag and $\overline{H-K_{res}}$ greater than 0.23. We have indicated the nominal centers of the Lynds dark clouds inside the $\overline{H-K_{res}}$ = 0.23 mag confinement. The triangle indicates the location of HD 39572, an unreddened B9 star located at $199\pm^{55}_{33}$ pc as measured by Hipparcos. (b) This frame shows the variation of $\overline{H-K_{res}}$ with latitude including stars with σ_{JHK} ≤0.080 and is used for estimating the lower limit for the cloud confinement $\overline{H-K_{res}}$ = 0.23 mag. The vertical markers show the sequence LDN 1622, 1621, 1617 and 1624 (left to right). (c) Extinction - distance pairs for stars in reseaus with $\overline{H-K_{res}}$ > 0.23 mag and with σ_{JHK} < 0.040 mag. The triangle locates HD 39572 having assumed that its a MS star. The solid curve indicates the arctanh fit $D_{LDN1622}$ = 233±28 pc to the sample confined by D_{max} = 350 pc

LDN 1634 found by Bally et al. ([2009]).

4.5 The Lupus Region

The Lupus clouds have a complex distribution on the sky and may be overlapping. We are therefore in need of a good confining procedure. As the maps by Cambrésy ([1999]) show optical star counts are useful to locate clouds but the reseau average of $(H-K)$ may be even better.

Lupus I – Lupus VI (Cambrésy ([1999]), form a complex covering a large region of the sky $\sim 10 \times \sim 15$ $\square^{\circ}$. The outline of the complex in integrated ^{12}CO intensities, A_K extinction and optical extinctions are given by Tachihara et al. ([2001]), Lombardi et al. ([2008]) and Cambrésy ([1999]) respectively.

The angular extent of the clouds alone suggests that the complex could be rather nearby. That is if the individual clouds are physically connected. Most often these clouds are understood as constituting a single spatial structure. If this is the case a single distance applies to all constituents. A small well defined isolated cloud may of course have its distance given by a single number. More extended features may be expected to have a depth comparable to their size on the sky. For Lupus this would mean a depth of approximately $2{\times}140{\times}tan(\sqrt{10\times 15}/2) = 30$ pc. The 30 pc also indicates the demands on the accuracy of the estimated cloud distance. Similar differences may accordingly be expected between individual cloud distances. In a detailed study of the kinematics of PMS stars in the Lupus Association Makarov ([2007]) demonstrated that the distribution of star formation during the past $\approx$25 *Myr* has had a depth of more than $\approx$30 pc. Roughly identical to the linear projection on the sky. The depth of the Lupus complex has also resulted from a maximum likelyhood analysis of photometric and astrometric data for the Ophiuchus and Lupus regions, Lombardi et al. ([2008]). Suggesting a thickness of Lupus of 51^{+61}_{-35} pc. The thickness likelyhood of the Lupus complex indicates that the depth may extend to somewhat beyond 200 pc.

With a proper distribution of stars in the A_V *vs. distance* plane or rather in the $H-K$ *vs.* $J-H$ diagram we may obtain accuracies on the cloud distances from the curve fitting on the $\pm$10 pc level and may accordingly distinguish a cloud at $\approx$150 pc from one at $\gtrsim$200 pc.

Apart from Lupus V the Lupus clouds have an elongated, filamentary appearence and are separated by regions with low or almost no extinction. Lupus I and II seem to be isolated from each other and from the 4 other clouds by low extinction space, e.g. Cambrésy ([1999]). Since the latitude of the complex is in the range from $b \approx 4^{\circ}$ to $b \approx 18^{\circ}$ we may expect to have a high but varying stellar density and we may have enough stars to confine the distance interval for the curve fitting from the variation of the distance averaged density n_H and its derivative $\delta n_H/\delta D_{\star}$. Generally we confine the discussion to stars with σ_{JHK} <0.040 mag. The size of the outlining $\overline{H-K_{res}}$ values vary from cloud to cloud partly caused by the latitude range but also by the extinctions in the various clouds. We identify the lower limit of $\overline{H-K_{res}}$ pertaining to the cloud sight lines from diagrams of $\overline{H-K_{res}}$ vs. one of the celestial coordinates, see e.g. Fig. 7 or 8. Note that the extinctions we discuss are below $A_V \approx$4.5 mag. Due to the limitations of our procedure we are not able to measure such large extinctions as the one given for the outer contour, $A_V \approx 8$ mag, in the discussion of Lupus III by Teixeira et al. ([2005]).

4.5.1 Lupus I

Fig. 9 shows how the perimeter of Lupus I, as defined by the average $(H-K)$ color, changes its appearence when the lower limit is varied from 0.15 to 0.18 whereas the appearence only changes marginally when the limit is raised to 0.19 or 0.20. A comparison of Fig. 9 to the optical or infrared extinction maps shows a good agreement, even for minute details. As several other dark clouds Lupus I has low extinction arcs protruding from its main body.

One could imagine that the *distance vs.* A_V diagrams would depend on the photometric error σ_{JHK}. But applying samples with σ_{JHK}=0.08 and σ_{JHK}=0.04 respectively demonstrates that this may not necessarily be the case for Lupus I. An eye fit of the cloud distance would indicate 100 – 150 pc in both cases. The extinction rise is clearly defined by the sample in reseaus with $\overline{H-K_{res}}$ >0.20 and $\sigma_{JHK} < 0.040$. Confining the sample by these limitations and with D_{max}=250 pc in the $arctanh^p(D_{\star}/D_{cloud})$ fit we obtain $D_{LUP\ I}$=144±11 pc as

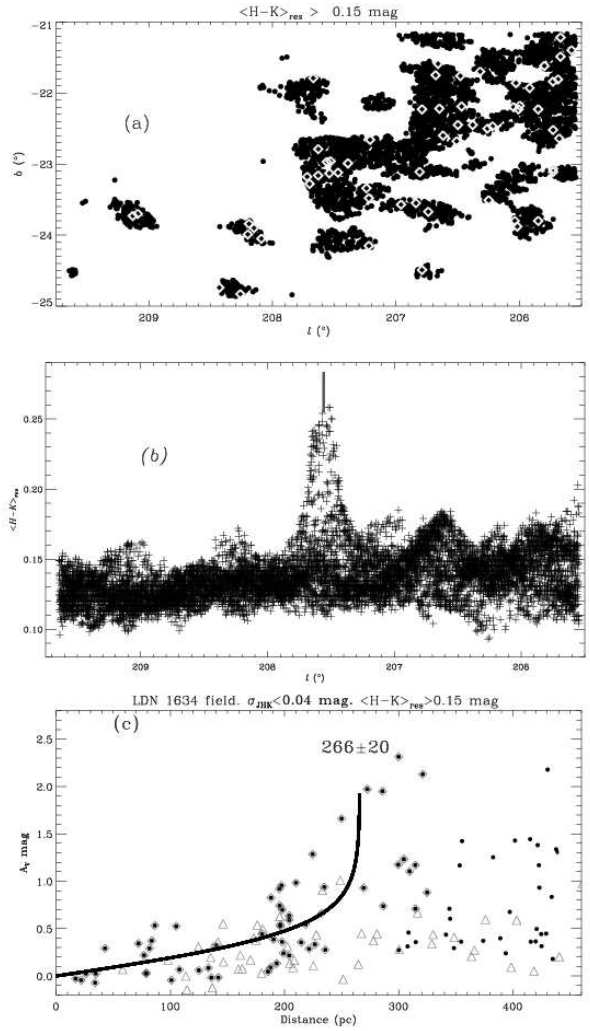

Figure 8: The LDN 1634 area. (a) Collection of stars with σ_{JHK} ≤0.040 mag and $\overline{H-K_{res}}$ greater than 0.15 from a 4×4 □° centered on (l, b) = (207.6°, -23.0°). Diamonds is the sample used for the distance fit. (b) This frame shows the variation of $\overline{H-K_{res}}$ with longitude including stars with σ_{JHK} ≤0.080. The vertical marker shows the longitude of LDN 1634. (c) Extinction - distance pairs for stars in reseaus with $\overline{H-K_{res}}$ > 0.15 mag and with σ_{JHK} < 0.040 mag. The solid curve indicates the arctanh fit $D_{ldn1634}$ = 266±20 pc to the sample confined by D_{max} = 425 pc. The points inscribed in diamonds is the sample used for the distance fit. Open triangles are the resulting extinction – distances variation for stars with Hipparcos parallaxes present in the area shown in panel (a) and for which spectral and luminosity were available in the literature. Their extinctions are estimated independently from 2mass data.

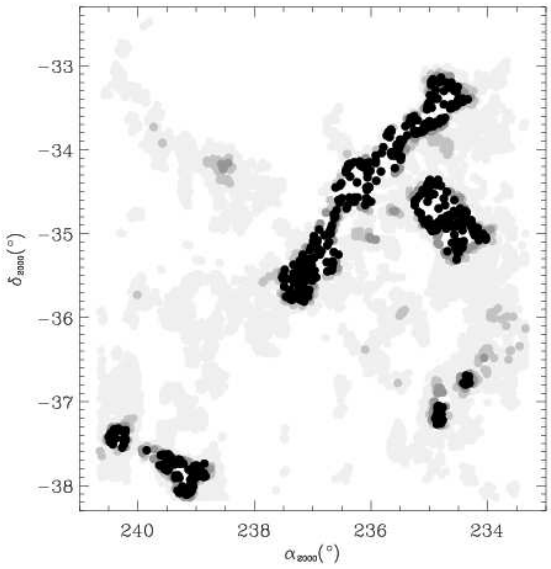

Figure 9: Lupus I region with an almost perfect match to the optical extinction map by Cambrésy. $\overline{H-K_{res}}$ >0.15, 0.18, 0.19 and 0.20 mag given. The triangular feature at the lower left is Lupus II. $D_{LUP\ I}$ = 144±11 pc

plotted in Fig. 10. In their March 10, 2008 c2d synthesis of Lupus Merín et al. ([2008]) quote 150±20, suggested by Comerón ([2008]) in his review of the Lupus complex, as a reasonable Lupus I distance.

4.5.2 Lupus II

Lupus II is included in the lower left part of Fig. 9 where it appears as an isolated feature between Lupus I and Lupus III - Lupus IV. We have previously attempted to estimate its distance, Knude and Nielsen ([2001]), from V and I photometry. The $(V-I)$ distance estimate was rather large, 360 pc, but was corroborated to some extent by Hipparcos data for four stars, 353 pc, with a relative precision of 30%. Since the extent of the cloud is small we include stars with $\sigma_{JHK} < 0.060$ and the cloud outline is again defined by $\overline{H-K_{res}} > 0.20$ mag. The distance fitted becomes 191±13 pc. Significantly larger than $D_{Lupus\ I}$ = 144±11 pc but smaller than the $(V-I)$ estimate.

4.5.3 Lupus III

The projection of Lupus III shows this cloud to be one of the minor components of the Lupus complex and on Cambrésy's extinction map Lupus III appears as an appendix to the apparently coherent feature consisting of Lupus IV, V and VI. The densest cores of Lupus III, forming the bridge head of the filament protruding from the Lupus V and VI combination, was discussed by Teixeira et al. ([2005]) in a study of the physical parameters of the clumps with star forming activity and those without. We divide the Lupus III region in the three subareas A, B and C indicated in Fig. 11. The subarea C contains the concentration of newly formed stars. The distance to this region is particularly important for estimating parameters used to study the star forming process.

It turns out that Lupus III as outlined by optical extinction by Cambrésy does not have a unique distiance. The extinction contours appear to be a projection of two superposed clouds. The estimate of the A area is $D_{LUP\ III_A}$ = 205±5 pc compared to $D_{LUP\ III_B}$ = 155±3 pc. The small C area covering the dense cores of Lupus III contains fewer stars partly because the area is small and partly due to the larger extinction of the dense core but as Fig. 12 shows we probably do have enough stars for the distance estimate. The curve fitting returns the estimate $D_{LUP\ III_C}$ = 230±21 pc in concord with $D_{LUP\ III_A}$ but significantly different from $D_{LUP\ III_B}$. The

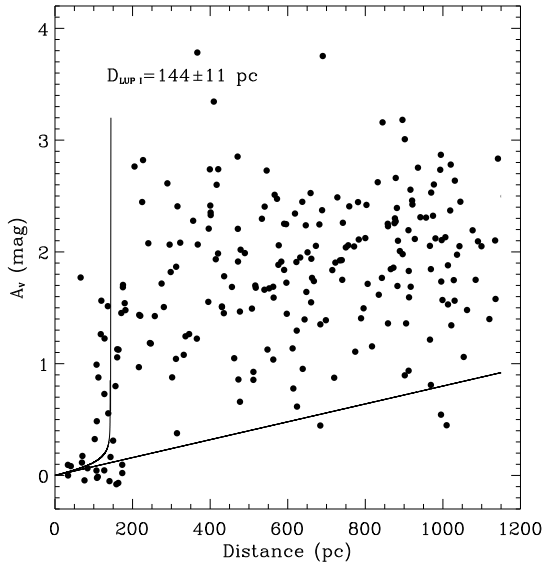

Figure 10: Lupus I region. Stars with σ_{JHK} < 0.040 mag and inside the $\overline{H-K_{res}}$ = 0.15 perimeter

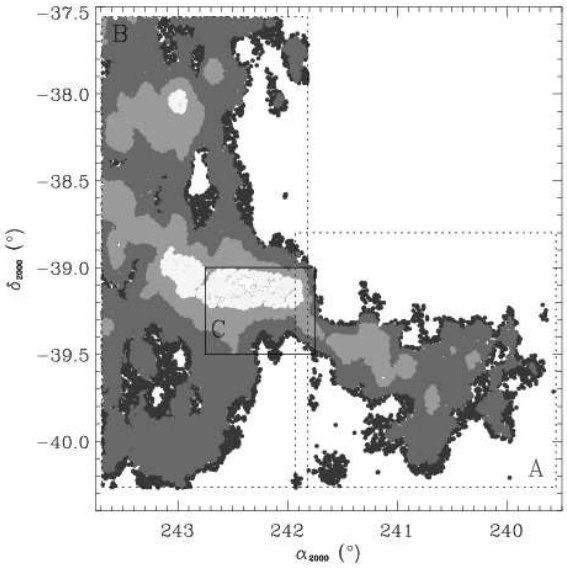

Figure 11: Distribution of the $\overline{H-K_{res}}$ > 0.18, 0.20, 0.25, 0.30 and 0.35 reseaus. The A, B, and C boxes for which stellar distances and extinctions are estimated are shown. The C-box corresponds to the region studied by Teixeira et al. ([2005])

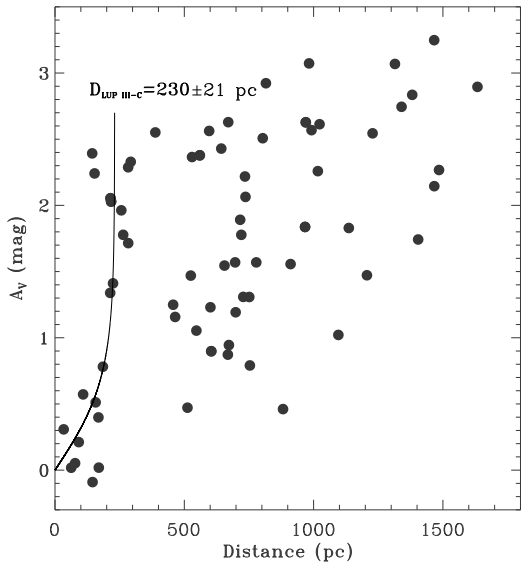

Figure 12: Lupus III-C region: $\alpha_{2000} \in [241.75, 242.75]$ and $\delta_{2000} \in [-39.5, -39.0]$. Sample limited by $\overline{H-K_{res}} > 0.18$ mag and only including stars with $\sigma_{JHK} < 0.040$ mag. $D_{LUP\ III-C} = 230\pm21$ pc

$D_{LUP\ III_C}$ distance is similar to the estimate for Lupus II of 191±13 pc. $LUP\ III_A$ and $LUP\ III_C$ are probably parts of the same physical structure located ≈50 pc behind the more extended $LUP\ III_B$. The distance difference is significant on the 3 – 5 sigma level and the distance estimates of the A+C and the B features have a releative precision ≲5%. Merín et al. ([2008]) quote 200±20 again as suggested by Comerón ([2008]) as a reasonable Lupus III distance consistent with our Lupus III_A and III_C estimates.

4.5.4 Lupus IV

Fig. 13 displays five $\overline{H-K_{res}}$ contours of this cloud roughly corresponding to $A_V \approx 0.5$, 1, 2, 3, and 3.5. Fig. 14 is showing distances and extinctions for stars within the $\overline{H-K_{res}} = 0.20$ contour. A comparison of Fig. 13 to Fig. 33 and Fig. 34, displaying the $\overline{H-K_{res}}$ and $count_{res}$ variation of ~ the same region of the sky, demonstrates the better capability of the reseau colors to bring out the cloud perimeter. The Lupus IV data permit $\overline{n}_H$ and $\delta\overline{n}_H/\delta D$ to be estimated so the sharp definition of the sample used for the curve fitting applies. The resulting cloud distance from the fit $D_{LUP\ IV} = 162\pm5$ pc. Lupus IV is also included in the c2d synthesis, Merín et al. ([2008]), where a Lupus IV distance 150±20 is quoted.

4.5.5 Lupus V

The projection of Lupus V is large, 4°×4° or more and Lupus III appears as an appendix to this cloud. A major part of the cloud is shown in the upper panel of Fig. 15. The middle panel of this figure shows a problem encountered when D_{max} is established from the variation of the line of sight density and does not display a sharp peak followed by a shallow drop off as expected from the template of Fig. 1(a) but a only shallow profile without the peak. The full width distance from a shallow profile would imply too large an estimate of D_{max} again implying too large a cloud distance. A possible interpretation of the density profile valid for the Lupus V area is that this cloud does not have a sharp spatial location but may possess a substantial depth smoothing the density peaks. Instead we estimate D_{max} from the derivative of the density or as a slightly different approach from the derivative of the median extinction. This latter derivative is also shown in the figure. The shape of the two derivatives happens to be rather similar in fact. With D_{max} from the half width of the derivatives the fitted distance to Lupus V becomes 162±11 pc. Interestingly Lupus III_B, Lupus IV and Lupus V are at identical

distances. The nearest part of Lupus III is located at the Lupus V distance with $D_{LP_{IIIB}}$ at 155±3 whereas Lupus III_A and Lupus III_C are are found beyond 200 pc. Our estimated distances suggest that Lupus III_B, Lupus IV and Lupus V are at a common distance of ≈160 pc. Estimating the angular diameter of the Lupus III_B, IV and V combination to ∼5°, e.g. from Cambrésy's optical extinction map the projected size on the sky is ∼14 pc comparable to the uncertainty ±11 pc in the distance fit. Apparently these clouds do not make up a sheet like feature.

Using the derivative of median extinction? Returning to the shallow distribution of the line of sight average density distribution we mentioned it possibly could be caused by a spread of Lupus V along the line of sight which somehow contradicts the common distance of Lupus III_B, IV and V. An extinction is of course the integrated effect of scattering and absorption along a sight line and must be related to the intregral of the particle number density along this sight line. If we assume that the median extinction is representative of this integrated particle distribution its derivative will represent a particle density – sort of an on the spot density contrary to the smooth average line of sight density. From the derivative of the median extinction shown in Fig. 15 we may possibly state that the corresponding density variation might be gaussian. We thus assume that our extracted sample probes a "feature" with a gaussian number density distribution. This "feature" is perhaps not to be perceived as a spatial structure since our extraction of 2mass data with distance estimate does not probe the most dense parts of a cloud. If we assume it is located at 162 pc and the density distribution has a standard deviation like the uncertainty ±11 pc. With these parameters the "feature" may mimic Lupus V. After integrating the gaussian distribution and assuming that the density outside the "feature" equals the constant intercloud density the extinction, when scaled to the range noticed for the median extinction, becomes as indicated in the bottom panel of Fig. 15. With the assumed gaussian density distribution the expected extinction follows the rise of the median extinction within ≲10 pc. We are not quite sure how the result of this small calculation should be interpreted because a single narrow gaussian does not quite agree with the shallow variation of the average line of sight density.

4.5.6 Lupus VI

Lupus VI is another example where the line of sight average density does not display as sharp a peak as expected. Its shallow profile is evident from Fig. 16 and again we use the derivative of either the density or of the median extinction. In Cambrésy's extinction map the densest parts of Lupus VI seem to continue into Lupus IV and this is reflected in the similarity of the Lupus VI distance 173±10 pc that does not differ from the 162±5 pc estimated for Lupus IV. Fig. 16 is a display of the Lupus VI data, the sample used for fitting a distance to the extinction jump and curves showing the variation of the median density and its derivative. The curve overplotted the median extinction has the ICM slope and may show the variation of the extinction originating in the intercloud medium beyond Lupus VI.

4.6 The Depth of the Lupus Complex

The debate on the proper distance to the complex of the Lupus I – Lupus VI clouds may be caused by measurements in components that have different distances and in particular the more shallow photoelectric measurements (e.g. Hipparcos and *uvbyβ*) may possibly not pertain to the molecular component but to the shells and sheets located in the solar vicinity.

We have collected our distance estimates in Fig. 17 together with the distance errors from the curve fitting. Apart from Lupus I, III_B, V all clouds are significantly more distant the canonical distance 140 – 150 pc. Including the 8 cloud components of Fig. 17 the maximum cloud separation is $\text{Lupus}_{\text{depth}}$ ≈86±24 pc. Excluding Lupus III_C the depth narrows to $\text{Lupus}_{\text{depth}}$ ≈ 60±12 pc. The estimated depth is accordingly about three times the projected size ≈26 pc at 140 pc.

A simple mean of the eight distances becomes 178±3 pc where the 3 pc is the error of the mean. At 173 pc the projected width becomes ≈32 pc still less than the extent along the line of sight. In a recent review of

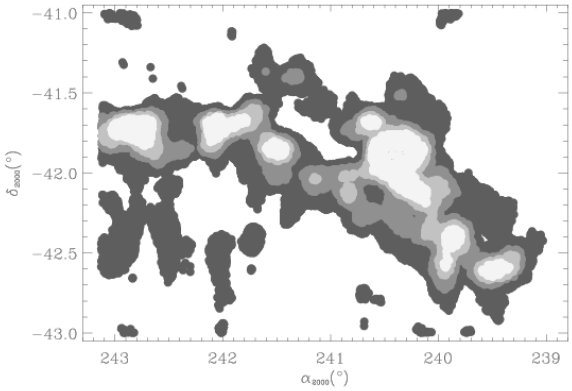

Figure 13: $\overline{H-K}$ contours of Lupus IV defined by $\overline{H-K_{res}} > 0.16, 0.20, 0.25, 0.30, 0.35$ mag inside the respective outlines. The boundary correspond approximately to $\overline{A_V} \gtrsim 0.5, 1.1, 1.9, 2.7, 3.5$ mag. This diagram may be compared to Figs. 33 and 34 where contours given by the reseau counts are shown. The three eastern most clumps with $\overline{H-K_{res}} > 0.30$ are discernible in Fig. 34

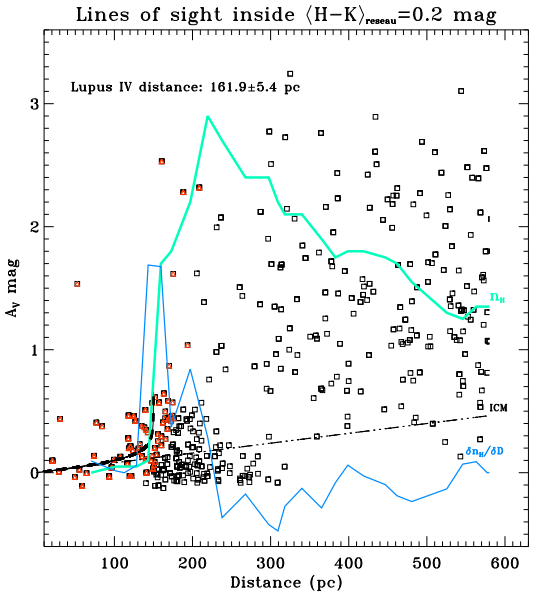

Figure 14: A_V *vs.* D diagram for the Lupus IV cloud shown in the previous figure. Arbitrarily scaled curves showing n_H, $\delta n_H/\delta D_{bin}$, ICM together with the curve fitted to the extinction jump. Only stars in reseaus with $\overline{H-K_{res}}$ exceeding 0.20 mag. Resulting cloud distance 162±5 pc

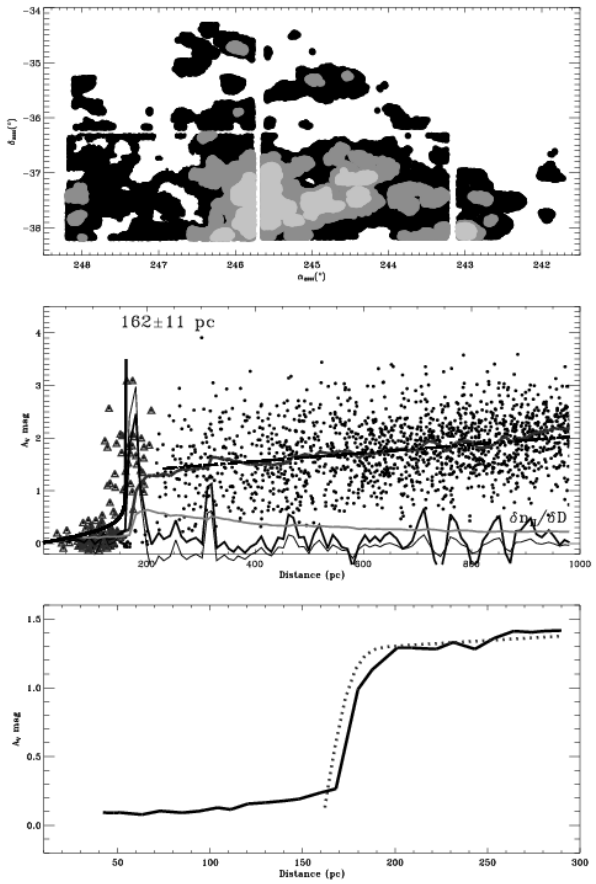

Figure 15: LUPUS V. *Upperpanel* area for which 2mass data with $\sigma_{JHK} < 0.040$ have been extracted. Outer contour corresponds to $\overline{H-K_{res}} = 0.20$, the next to 0.025 and the innermost to 0.30. The *middlepanel* is the A_V *vs*. D diagram complemented with some statistics. The lower thin curve is an arbitrarily scaled display of $\delta n_H/\delta D_{bin}$ used to estimate D_{max}. The lower smooth curve is the mean line of sight density arbitrarily scaled. The median extinction is also shown and the dashed line overplotted the median represents the ICM variation. Only stars in reseaus with $\overline{H-K_{res}}$ exceeding 0.20 mag equivalent to $A_V \gtrsim 1.9$ mag. Resulting cloud distance 162±11 pc is based on stars with $\sigma_{JHK} < 0.040$ and located in reseaus where $\overline{H-K_{res}} > 0.20$. The *bottompanel* shows the comparison of the median extinction and the extinction resulting from a cloud with a gaussian density distribution centered on D_{LPV}=162 pc and with σ=11 pc

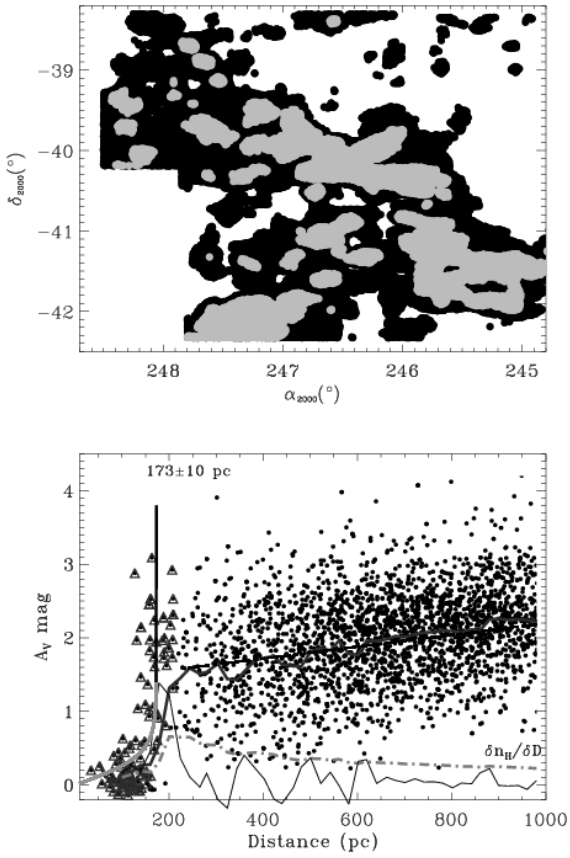

Figure 16: LUPUS VI. *Upperpanel* shows area for which 2mass data with $\sigma_{JHK} < 0.040$ have been extracted. Outer contour corresponds to $\overline{H-K}_{res} = 0.25$, the next to 0.030. The *lowerpanel* is the A_V *vs*. D diagram. The lower smooth curve is a scaled line of sight density. The lower thin curve is an arbitrarily scaled display of $\delta n_H/\delta D_{bin}$ used to estimate D_{max}. The median extinction is also shown and the dashed line overplotted the median represents the ICM variation. Only stars in reseaus with $\overline{H-K}_{res}$ exceeding 0.250 mag equivalent to $A_V \gtrsim$1.9 mag. Resulting cloud distance 220±10 pc is based on stars with $\sigma_{JHK} < 0.040$ and located in reseaus where $\overline{H-K}_{res} > 0.25$

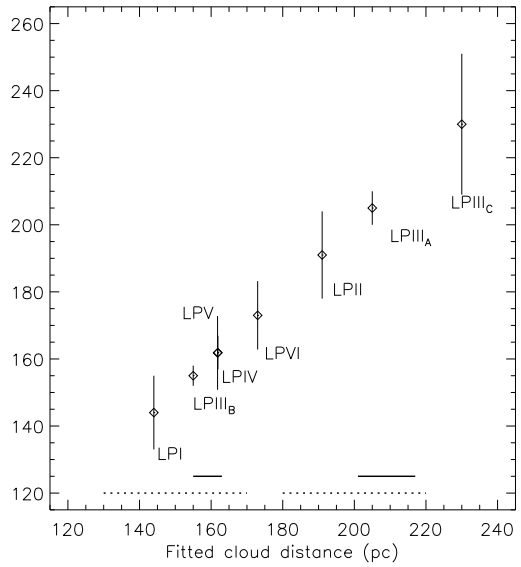

Figure 17: Resulting distances for the Lupus I-VI clouds with errors indicated for the individual cloud components. Lupus IV and V have identical distance estimates and Lupus III is made up of components at two significantly different distances. The dotted lines indicate the reasonable distance ranges for Lupus I, IV and Lupus III suggested by Comerón ([2008]) and the ranges, 159±4 and 209±8 pc respectively, are the mean±error of the mean distance that we suggest for the nearby and remote group of clouds

the Lupus complex Comerón ([2008]) concludes that Lupus I and IV is at 150±20 pc, Lupus III at 200±20 pc. From our results in Fig. 17 we notice that $D_{LUP\ I}$=144±11 pc is compatible with a distance of 150 pc and that $D_{LUP\ IV}$=162±5 pc seems to be marginally larger than 150. But for Lupus III only the A and C components, see Fig. 12, with distances 205±5 pc and 230±21 pc are at ~200 pc whereas the B component is at ~150 pc.

Taking Lupus I, III$_B$, IV, V, VI as a common feature and Lupus II, III$_A$,III$_C$ as a separate structure the first group has a mean distance 159±4 and the second 209±8 pc consistent with the suggestion from Comerón's ([2008]) review. Perhaps the two groups should not be considered as spatially connected?

According to Tachihara et al. ([2001]) Lupus III displays the largest velocity dispersion of the Lupus I – VI clouds indicating a possible distribution along the line of sight.

4.7 The Chamaeleon Clouds

For the Chamaeleon clouds, Luhman et al. ([2008]), quotes 162 pc for the Cha I distance. In Luhman ([2008]) the best Cha I distance estimate is adopted to be in the range 160 – 165 pc. The Cha II estimate is given as 178±18 pc adopted from Whittet et al. ([1997]) and is marginally larger than the Cha I distance. No estimates are given for Cha III in the review by Luhman ([2008]). In their study of nearby molecular clouds, Knude and Høg ([1998]), detect the first indications of an extinction jump in the Chamaeleon region reaching $A_V \lesssim 1$ mag at a distance ≈150 pc based on about 10 stars. This distance seems consistent with the 160 – 165 pc quoted by Luhman ([2008]). For the discussion of the Chamaeleon distance estimates the data and results are given in the panels of Fig. 18.

4.8 A 3×3 □° region comprising Chamaeleon I

Being rather nearby and accomodating active, star formation with a model median age ≈2 Myr, Cha I is a well suited cloud to search for low mass starsa and brown dwarfs still possessing their disks, Luhman et al. ([2008]), Luhman and Muench ([2008]). Membership of the Cha I star forming clusters was based on three criteria of

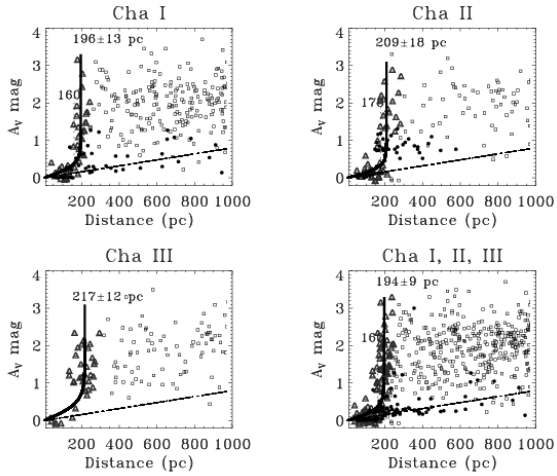

Figure 18: Data and distance estimates for the three Chamaeleon clouds. In the frame to the lower right we have combined the data for the three clouds with a resulting distance etimate $D_{Chamaeleon}$ =194±9 pc. Apart from the lower left panel the panels contain the photometric data (small filled circles) from Whittet, Prusti, Franco et al. ([1997]) measured for Cha I and Cha II

which distance is just one. Distance in the sense that a candidate must be placed above the main sequence when shifted to the distance (and extinction) of Cha I. The outer contours corresponding to $\overline{H-K}_{res}$= 0.2 mag is similar to the contours given in Fig. 1 of Luhman and Muench ([2008]). From the variation of $\overline{n}_{H,los}$ with distance we estimate D_{max} and the arctanh fit returns $D_{Cha\ I}$ = 196±13 pc. Data and fit are given in Fig. 18 together with Whittet et al.'s ([1997]) estimate of 160 pc. In the Cha I frame of Fig. 18 the filled black circles indicate Whittet, Prusti and Franco, et al.'s data ([1997]) and they are seen to follow our data closely. The 160 pc line appears as a lower distance limit to the jump rather than a fit. Changing the Cha I distance from 160 to 193 pc will increase $log\frac{L}{L_\odot}$ with 0.4 and as a consequence reduce the age estimate to make it coeval to Taurus (1 Myr), Fig. 11 of Luhman ([2008]). If the larger distance is accepted it influences our understanding of the disk life times. The two distance estimates differ only on the 2 sigma level.

The filled circles of the Cha I and II panels of Fig. 18 indicate the data from Whittet et al. ([1997]) and we notice that the largest extinctions pertaining to the jump falls within the distance range of the stars we have used for our curve fitting. The less extincted stars of Whittet et al. follow the ICM curve very well.

4.9 A 2×2 □° region centered on Chamaeleon II

Chamaeleon II is a nearby star forming cloud and Porras, Jørgensen, Allen et al. ([2007]) presented Spitzer IRAC data for parts of Chamaeleon II where $A_V > 2$ mag. We have drawn the 2mass data for a similar 2×2 □° box region centered on (l, b) = (303°,-14°) and with $\sigma_{JHK} \leq 0.080$ mag.

Whittet, Prusti, Franco et al. ([1997]) present the photometric distance to Chamaeleon II as 178± 18 pc whereas Knude and Høg ([1998]) suggest 150 pc for the greater Chamaeleon region.

In the 2×2 □° we extract stars located in reseaus with $\overline{(H-K)}_{reseau} > 0.2$ mag. We apply the variation of the line of sight average density to define the stellar sample used for fitting the arctanh function. The resulting distance is estimated to $D_{Cha\ II}$ = 209±18 pc and is shown in Fig. 18 together with data used by Whittet et al. ([1997]) for their distance 178 pc. The 178 pc almost appears as a lower distance limit for our cloud sample and coincides with D_{fit}-σ_{fit} = 191 pc when we recall that in the optical gooda individual photometric distances have a precision in the range 20% - 30%.

4.10 The Chamaeleon III cloud

For the sake of completeness the Chamaeleon III cloud is included moreover because its distance has not been discussed to the same detail as the Cha I and Cha II distances. Again the cloud is confined by $\overline{H-K_{res}}$= 0.20 mag but now with $\sigma_{JHK} < 0.040$. We estimate the distance to $D_{Cha\ III}$ = 217±12 pc. There is, however, a strange lack of stars between 250 and 350 pc so the $\overline{n}_{H,\ los}$ peak may be artificially narrow. Considering the standard deviation of the stellar distances the eye would probably locate the cloud at 200 pc but with the cloud fitting sample based on D_{max}=350 pc from the $A_V/D_\star$ variation the fitted distances becomes slightly larger.

Since the three distances 193±13, 209±18 and 217±12 pc respectively, are identical within the errors we combine the data with $\sigma_{JHK} < 0.040$ and $\overline{H-K_{res}} > 0.20$ for all three clouds. The common distance becomes 194±9 pc which is shown in the lower right panel of Fig. 18. In this panel we also notice how well the minimum extinction beyond the cloud distance follows the diffuse intercloud extinction, A_V = 0.008 mag/100 pc from Knude ([1979b]), and this includes the optical data from Whittet et al. ([1997]) as well.

4.11 DC300.2-16.9

This cloud, or infrared cirrus, is located between Cha I and Cha III and Whittet et al. ([1997]) assumes it is at the same distance as the Chamaeleon complex of clouds, ∼170 pc. A more recent multi-wavelength study of this cloud, Nehmé et al. ([2008]), argues that the cloud is associated to the T Tauri star T Cha and that its distance accordingly is as small as the stellar distance of a mere 70 pc. The area inside the contour $\overline{H-K_{res}} >$ 0.2 mag is less than one square degree and the sample is too small to allow a good distance determination. The tail of this cometary cloud, Nehmé et al. ([2008]), extends several degrees towards the south and has a most patchy $\overline{H-K_{res}}$ distribution with 3 – 4 apparently denser concentrations. If we relax the density requirement to $\overline{H-K_{res}} > 0.16$ mag which includes the concentrations in the tail as well. Five stars with $A_V > 1$ mag and distances between 90 and 140 pc define an uprise of extinction closer than 150 pc. Their average distance is 118±24 pc and the average extinction amounts to A_V = 1.3±0.3 mag. This is by no means conclusive but may indicate that DC300.2-16.9 is on the nearer side of the three Chamaeleon clouds. From an extensive *uvbyβ* survey of the general Chamaeleon region Corradi, Franco and Knude ([1997]) found evidence for a dusty sheet between 100 and 150 pc which may contain the infrared cirrus DC300.2-16.9.

4.12 The Musca cloud

The Musca cloud is located only ≈4 degrees closer to the galactic plane than Chamaeleon II and may have been formed together with the Chamaeleon clouds, Corradi, Franco and Knude ([2004]), making its distance interesting to know. From stars in reseaus with $\overline{H-K_{res}}$ exceeding 0.20 mag and with $\sigma_{JHK} < 0.040$ the resulting distance is 171±18 pc slighly less than the three Chamaeleon clouds, but only by a one sigma difference.

4.13 The Southern Coalsack

Despite the Coalsack lacks star forming activity but does contain dense globules its distance may be interesting. Estimates of the Coalsack distance range from 150 to 200 pc and were summarized by Andersson et al. ([2004]). Its location close to the galactic plane assures a high stellar density for the extraction of usable data. We extracted data with $\sigma_{JHK} < 0.04$ mag in 9 box regions with centers located along the outer CO contour of 2 $K\ km\ s^{-1}$ and sides ranging from 1.5° to 3.0°. Their location and size are given in Table 1. From the distance variation of the average density a D_{max} is assigned to each sub-region and distances are estimated in the range from 140 to 220 pc for the separate fields and they are given Table 1 together with their standard deviations. The distances are estimated on the ≲10% level. When all the data are combined the fitting procedure returns $D_{Coalsack}$ = 174±4 pc. The unphysical goodness of the fit is due to the large number of available data points. Unphysical because the distance separation between the 140 and 221 pc valid for the closest and remotest cloud (in our extraction) seems significant. With an angular diameter of 15° the estimated projected size is about 45

Table 1: Distance to nine individual regions in the Southern Coalsack and the distance, 174±4 pc, from the combined data

Region	Size	long.	lat.	D_{cloud}	$\sigma_{D_{cloud}}$
	$\prime \times \prime$	$^\circ$	$^\circ$	pc	pc
I	90×90	304.5	+0.5	140	7
II	100×100	301.5	+0.5	190	15
II_b	100×100	303.0	-1.0	208	12
II_c	100×100	303.0	+1.0	203	11
III	100×100	304.5	-1.5	213	10
IV	90×90	301.5	-2.5	175	12
V	120×120	299.5	-4.0	221	13
VI	120×120	306.0	-4.0	209	15
VII	120×120	306.0	-1.5	160	13
Combined				174	4

pc. There has been a discussion, based on sparse data though, whether the Coalsack consisted of two clouds, see Andersson et al. ([2004]). Whether there are two or more clouds is corroboated by the depth noticed in the few regions we studied.

Fig. 19 shows the median extinction calculated in 20 pc wide bins with a 50% overlap with their neighours. The 174 pc fit is also shown together with the range of distances displayed by the individual regions. Behind the extinction jump is shown the variation from the diffuse intercloud medium shifted by 0.5 mag. The coincidence with the median extinction may support the presence of a void beyond the Coalsack or it may not since a ∼magnitude limited sample will fail to measure distant dense clouds.

It is, however, interesting to compare the variation of the median extinction of the Coalsack to the one we derived for Lupus V, Fig. 15 where the intercloud slope seems applicable immediately behind Lupus V. For the Coalsack on the other hand the intercloud slope only fits the median of the combined data ≈300 pc beyond the assigned distance of 174 pc and it starts at a median extinction ≈0.3 mag below the peak. This may possibly be taken as an effect of a somewhat patchy density distribution in the Coalsack, at least in the data we have extracted, and a distribution of clouds along the sight line.

4.14 The Circinus molecular cloud complex

The Circinus region, composed by several dark clouds, were searched for $H\alpha$ emission stars by Mikami and Ogura ([1994]) suggesting concentrations of emission line stars at the outlines of the clouds DCld 318.8-4.4 and DCld 316.9-3.8 that have the largest galactic longitudes. Compared to other molecular clouds the Circinus clouds appear much more frayed. An appearance ascribed to the combined effect of the outflows of previous and ongoing star formation, Bally et al. ([1999]). No dedicated efforts to estimate the Circinus clouds distance were found in the literature but from the Neckel and Klare ([1980]) catalog Bally et al. ([1999]) quote an extinction increase to A_V ∼0.5 at ∼170 pc and a second jump to more than 2 mag between 600 and 900 pc. In Fig. 20 we have plotted Neckel and Klare's stars from a 5°×5° region centered on the Circinus cloud together with our results. Distances and extinctions of Neckel and Klare's stars are mostly based on a MK classification. We have extracted the 2mass data for five 1°×1° regions covering the apparently densest parts of the complex. Confining the sample to stars located in reseaus with $\overline{H-K}_{res}$ exceeding 0.35 mag and with $\sigma_{JHK} < 0.040$ mag we end up with the diagram shown in Fig. 20. Bally et al. ([1999]) discuss the location of the complex within 170 and 900 pc. We note that the 'wall' at 170 pc also appears in our data beyond ∼200 pc but also that

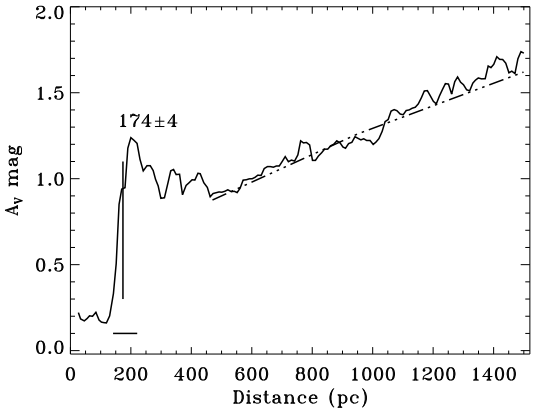

Figure 19: The Southern Coalsack. The solid curve shows the median extinction in 20 pc wide distance bins resulting from the combined Coalsack data. The vertical solid line indicates the distance resulting from the curve fitting and the horizonthal line the range of cloud distances in the nine individual fields. The dashed line is the expected variation caused by the diffuse intercloud medium shifted by 0.5 mag.

an extinction rise appears on the near side of 600 - 900 pc as indicated by a $A_V \approx 0.5$ mag shift in the run of the intercloud ISM, indicated by the shift of the line labelled ICM in Fig. 20. The curve fitting suggests a distance 436±29 pc somewhat smaller than the 700 pc adopted by Bally et al. Fig. 20 further indicates that the lower envelope follows the general ICM slope but also that a shift of the lower envelope may take place at ~800 pc. 436 pc is almost within the factor of 1.5 suggested as the uncertainty on the previously suggested distance of 700 pc, Bally et al. ([1999]). Reducing the cloud distance to 436 pc will reduce mass, linear momentum and kinetic energy estimates by a factor ≈0.4 whereas dimensions and dynamical ages will be smaller by ≈0.6. The reduction of linear dimensions will reduce the size of all the outflows to $\lesssim$1 pc. More interestingly perhaps, the star formation efficiency given by Bally et al. will be increased by ≈1/0.4 implying η_{SFE}=3-20% counting only the four most massive stars and η_{SFE}=12.5-50% including the sources of all ten outflows. These efficiencies are rather high, the upper limits (20 – 50%) almost at the level valid for star forming cores, which may be right since the Circinus clouds may be remnants left after intensive star formation. According to McKee and Ostriker ([2007]) the star formation efficiency is ≈5% averaged over the lifetime of a cloud.

4.14.1 DC 314.8-05.1. An isolated globule or associated to the Circinus complex?

DC 314.8-05.1 is only removed a few degrees from the Circinus complex and may be an example of a small isolated molecular cloud showing significant extinction but possibly without star formation. A particular reason for discussing this cloud is that it , Whittet ([2007]), had it distance estimate revised from ≈175 pc to 342±50 pc. Due to its minor size and large extinction optical estimates of distance and extinction may prove difficult. The 342±50 pc suggested by Whittet is based on reflection on the dark cloud of the light from an "associated" B star and a larger than standard value of R_V=4.25 possibly justified by grain growth in dense environments of the globule. The stellar distances we use are all based on our standard reddening law. The 170 pc distance estimate is again based on the catalog by Neckel and Klare ([1980]), see Fig. 7 of Whittet where an extinction rise is noticed at about 200 pc, as was the case for the Circinus region, and a second jump at about 700 pc. From 2mass we extracted stars within a 1°×1° region centered on the globule. The extinction – distance data are only based on lines of sight with $\overline{H-K_{res}}$ exceeding 0.2 and $\sigma_{JHK} < 0.04$. The interpretation of the resulting extinction

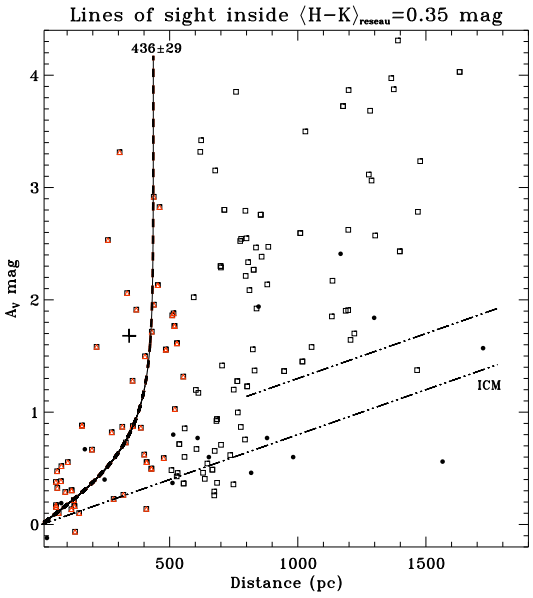

Figure 20: Circinus. A_V *vs*. D diagram for a ~5□° region composed by 5×1□° areas covering the denser parts of the Circinus complex, e.g. the $H\alpha$ emission stars in DCld 318.8-4.4 and DCld 316.9-3.8. For comparison we show the filled dots representing distance(MK) vs. A_V(MK) from Neckel and Klare ([1980]) in a larger 5°×5° region centered on the Circinus cloud. Only stars with $\overline{H-K_{res}}$ exceeding 0.35 mag and with $\sigma_{JHK} < 0.040$ are included in this diagram. For comparison Whittet's ([2007]) distance to the nearby globule DC314-05 based on a distance estimate of HD 130079 is indicated with a cross at 342 pc. See separate discussion of this other cloud but with only a one sigma difference between the Circinus and DC314-05 distances DC314-05 could be physically associated to the Circinus complex?

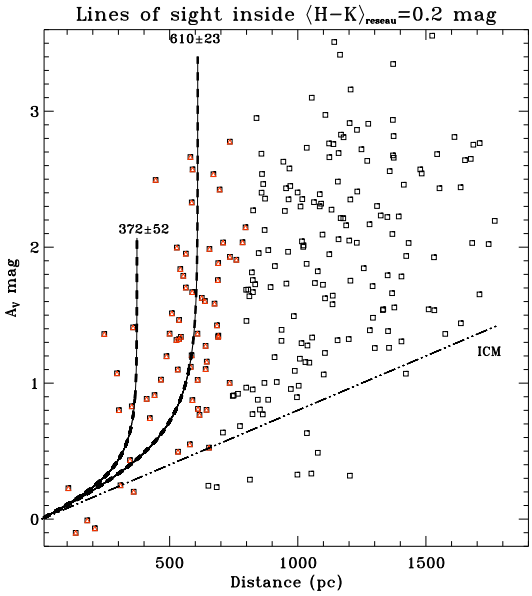

Figure 21: A_V *vs.* D diagram for a 1°×1° region centered on DC 314-05. Only stars with $\overline{H-K_{res}}$ exceeding 0.2 and $\sigma_{JHK} < 0.040$. $D_{DC\ 314-04}$ = 610±25 pc. Whittet's ([2007]) distance based on HD 130079, that is reflected on DC 314.8-05.1, amounts to 342±50 pc

– distance diagram of Fig. 21 is not simple since there are indications of two jumps and we may not be certain whether the apparent absence of stars between these two jumps is real or is caused by leaving out the M0 – M4 dwarfs. If caused by the selection effect the distant jump should be neglected. The first jump is at 372±52 pc and a second one at 610±25 pc. There is no sign of the rise at 170 pc in Neckel and Klare's data, which is based on a single star anyway. Whittet suggests that R_V=4.25 for DC 314.8-05.1 and since we have been using the standard reddening law the use of a larger value of R_V implies a shorter distance than our suggested 372±52 pc. Comparing the DC 314.8-05.1 distance 372±52 pc from the literature to what we suggest for the Circinus complex 436±29 pc it may not be possible to maintain that DC 314.8-05.1 is isolated and not associated to the nearby Circinus complex. To corroborate this possibilty we indicated Whittet's distance determination for DC 314.8-05.1 in the Circinus extinction – distance diagram, Fig. 20.

4.15 IC 5146. A more distant cluster and cloud

Extinction and molecular gas in a dark cloud near the cluster IC 5146 was discussed in a seminal paper by Lada et al. ([1994]) and the cloud structure was investigated in more detail by a deeper H, K survey suggesting extinctions above A_V ∼20 mag, Lada, Alves and Lada ([1999]). The distances to the cloud and cluster, which can not be assumed to be identical *a priori*, are of some interest since the molecular filament studied by Lada et al. shows a σ_{A_V} vs. A_V variation and that the volume density falls off like r^{-2} over scale lengths in the range 0.07 – 0.4 pc assuming a distance of ∼460 pc. The σ_{A_V} vs. A_V variation was shown to be a consequence of the volume density variation $\sim r^{-2}$ and not a result of the supersonic tubulence model proposed by Padoan, Jones and Nordlund ([1997]). The young cluster IC 5146 contains a multitude of H_α emission stars, Herbig and Dahm ([2002]). Despite an angular separation ≈1.3° on the sky, see Fig. 22, it has been assumed that filament and cluster are at the same distance. The filament distance was first asumed to ≈400 pc by Lada et al. ([1994]) mainly due to a lack of foreground stars to the filament. In Lada et al. ([1999]) the estimate was changed to 460 pc with a one sigma range from 400 to 500 pc. These estimates are about half the distance estimated to the cluster IC 5146. Herbig and Dahm ([2002]) adopt what they term a compromise distance to the cluster of 1.2 kpc from estimates ranging from 0.9 to 1.4 kpc and quotes an uncertainty ±180 pc coming exclusively from the uncertainty of the M_V calibration of the three B8, B9 stars used to locate the V_0 *vs.* $(V-I)_0$ locus

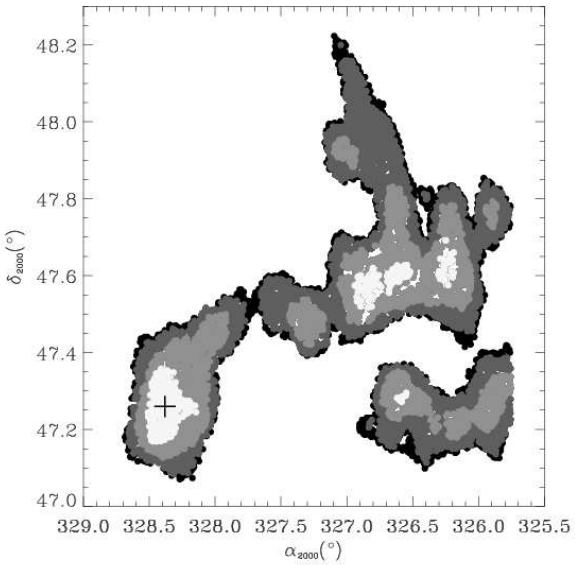

Figure 22: IC 5146. Projection of $\overline{H-K_{res}}$ = 0.21, 0.26, 0.31 and 0.34 mag respectively for the two areas searched for stars that may be used for the distance estimate. The plus sign indicates the position of the IC 5146 cluster. The filament approximately centered at $\delta \approx 47.5$ and α in the range from 326 to 327° is the cloud discussed by Lada et al. ([1994]). Note that the angular separation between this filament and the IC 5146 cluster is about 1.3°

pertaining to the Pleiades and thought to represent the IC 5146 main sequence as well. Harvey et al. ([2008]) use a similar technique on B type stars projected on the cluster area and evaluate a new photometric distance by replacing the Schmidt-Kaler ZAMS by a newer luminosity calibration with data from the $\lesssim$1 Myr Orion Nebula Cluster which recently had a precise VLBA distance determination. Seven B-type stars are available, two were discarded on the grounds that they gave distances in the 300 – 400 pc range. Five late B-type stars provide an average distance module 9.89 mag with a standard error 0.18 mag implying the estimate 950^{+83}_{-75} pc for the IC 5146 cluster.

We have extracted 2mass data for the area shown in Fig. 22 and used the reseau mean of $(H-K)$ to indicate the extinction contours. In order to have enough stars for the reseau mean values we use stars with σ_{JHK} <0.1 mag somewhat larger than our preferred choice of 0.04 mag. The IC 5146 cluster position is indicated by the plus sign. From the mean color contours it is not obvious that the cloud filament and the cluster are parts of a coherent dust structure. Only a minor change of $\overline{H-K_{res}}$ from 0.20 to 0.21 breaks the color bridge from the cloud to the cluster. For the northern filament we extract stars with σ_{JHK} <0.05 mag and $\overline{H-K_{res}}$ >0.26 and $\alpha_{2000} < 327.5^\circ$. Distance-extinction pairs included for the curve fitting have a limiting distance D_{max} of 1000 pc. There are too few stars to define the distance range of the extinction rise from the variation of the mean density vs. distance. From Fig. 23 we notice how well the lower envelope is represented by the increase caused by the diffuse "intercloud" medium. The filament distance resulting from the fit is 603±65 pc corresponding to a ≈10% accuracy. The suggested distance to the cloud filament is roughly 2σ above the distance range 400−500 proposed by Lada et al. ([1999]). The scale length will change from 0.07−0.4 pc to 0.09−0.5 pc. Mass estimates will increase almost by a factor of 2 (∼1.7) if the increased distance estimate of 603 pc is accepted.

The area used to study the IC 5146 cluster region has $\alpha_{2000} > 327.5^\circ$ and is confined to 0.26< $\overline{H-K_{res}}$ <0.36. The upper confinement is chosen to avoid the inner parts of the cluster region where dust modifications may haven taken place and the colors may be influenced by warm dust emission. Fig. 24 shows the extinction vs. distance digramme for the "outer" parts of the cluster region. The fitting sample was limited by D_{max} = 1200 pc, increasing D_{max} to 1300 pc did not change the estimated distance 766±113 pc. The relative distance error

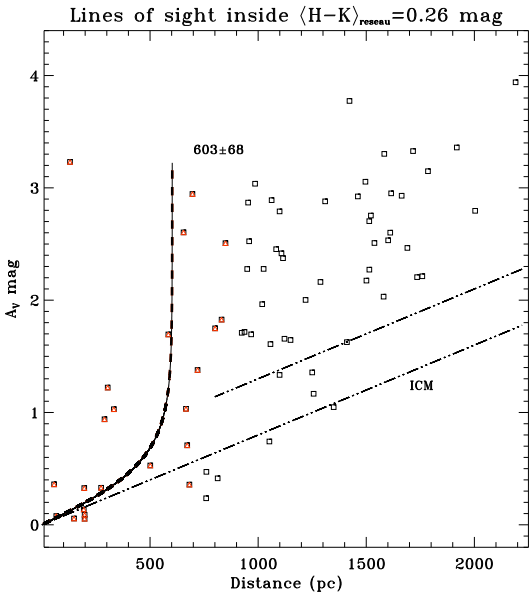

Figure 23: IC 5146, northern filament. A_V *vs.* D diagram from a 1.3°×1.3° region centered on the part of the IC 5146 clouds studied by Lada et al. ([1994]) where the NICE extinction estimate was introduced. Only stars with $\overline{H-K}_{res}$ exceeding 0.26, with $\sigma_{JHK} < 0.050$ and $\alpha_{2000} < 327.5°$ are included in the distance fit. A distance of 603±68 pc results

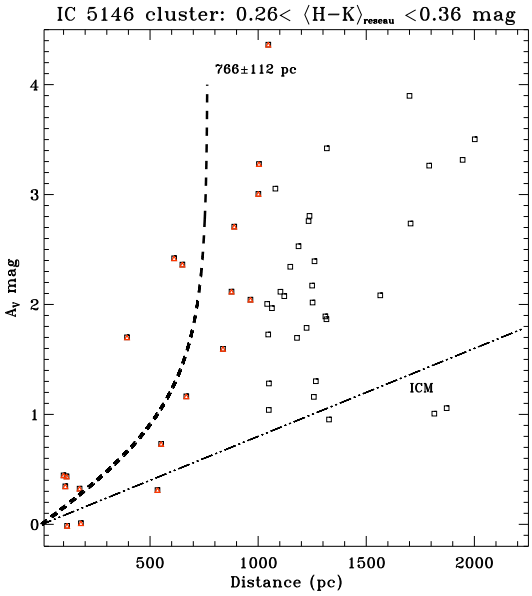

Figure 24: IC 5146 cluster. A_V *vs.* D diagram from a 1.3°×1.3° region containing the IC 5146 cluster. Only stars with $\overline{H-K}_{res}$ exceeding 0.26 but less than 0.36 and with $\sigma_{JHK} < 0.050$ are included. The upper limit is introduced to avoid the cental parts of the cluster and $\sigma_{JHK} < 0.050$ are included. Only stars with $\alpha_{2000} > 327.5°$ included. The distance of 765±112 pc results from fitting the $arctanh^p(D_\star/D_{cloud})$

is now gone up to 14% - really not bad for a feature possibly located at ~0.75 kpc.

The distance discrepancy between the northern dark cloud and the cluster remains but is narrowed from 460-1200 pc to 603-766 pc. The difference of our estimates is significant on the 2−3 sigma level. Taken at their face value and with a separation of 1.3° the filamentary cloud and the cluster will be separated by ≈163 pc and may accordingly not be physically related. Conversely Harvey et al. ([2008]) use circumstantial evidence to argue that cloud and cluster are at similar distances.

4.16 The Corona Australis Cloud

Compared to other star forming clouds Corona Australis has an isolated location at ~18° below the galactic plane and may have another formation history than most molecular clouds, Neuhäuser and Forbrich ([2008]). We have previously estimated the distance to the Corona Australis Cloud, Knude and Høg ([1998]), using Hipparcos parallaxes and color excesses including stars within 5° from (l, b) = (360.0, -20) and noticed a marked rise in the color excess at ~170 pc present in ≈15 stars with an estimated A_V range from 0.1 to 1.0 mag. In their isodensity maps of the local bubble Lallement et al. ([2003]) indicate a location of the CrA cloud at ≈120 pc. Three late B-type stars are close to the projection of the denser parts of the cloud and Neuhäuser and Forbrich ([2008]) suggest their Hipparcos parallaxes for a weighted mean 130 pc as the Corona Australis distance.

We have extracted 2mass data for this cloud with $\sigma_{JHK} < 0.040$ and limit the study to stars with $\overline{H-K}_{res}$ >0.15. The extraction with 0.15≤ $\overline{H-K}_{res}$ <0.16 is shown in Fig. 25 and is in fact a rather good representation of the optical extinction map from Cambrésy ([1999]). With D_{max} = 250 pc the resulting distance D_{CRA} = 148±13 pc. Fig. 25 also contains our previous estimate of 170 pc directly from the Hipparcos parallaxes and the location 130 pc recently suggested. The three stars on which the 130 pc distance is based display a low extinction and follow the general trend based on the 2mass data but is possibly underestimating the distance. Their relevance for the Corona Australis distance originates from the fact that they are likely to be CrA members.

4.17 LDN 1450, HH 7 - 11 or NGC 1333 in the Perseus Cloud

The dark cloud associated with the reflection nebula NGC 1333 hosts a number of pre main sequence stars, some even of the earliest classes 0 and 0/I, according to several authors, e.g. Chen, Launhardt and Henning ([2009]), Winston, Megeath, Wolk et al. ([2009]). Ages of these PMS stars range from 1 to 10 Myr with most objects being younger than 3 Myr. LDN 1450 appears to be associated to a complex of dark clouds reaching all the way to IC 348 – the Perseus Cloud. We have extracted 2mass data from a 4×4 □° area centered on (l, b) = (158.3°, -20.5°). We only include stars located in a reseau with $\overline{H-K}_{res}$ > 0.20 mag and $\sigma_{JHK} < 0.040$ mag. The distribution of lines of sight for which a distance – extinction pair could be computed is shown in Fig. 26(a) and the pairs displayed in the (c) panel together with the resulting estimate of the cloud distance $D_{LDN\ 1450}$ = 213±12 pc. D_{max} = 350 pc because the average line of sight density shows a rather wide distribution implying the large value of D_{max}. There exist an earlier estimate of the LDN 1450/NGC 1333 distance from Vilnius photometry in an area comparable to the one studied presently, Černis ([1990]). The Vilnius data are given for comparison in Fig. 26(b) and as smaller triangles in the (c) panel. The distance proposed from the Vilnius data is 220±20 pc and results from a weighting scheme including the most remote stars with $A_V < 0.7$ mag and the nearest ones with $A_V > 1.5$ mag. The agreement between the present estimate of 213 pc and the Vilnius estimate of 220 pc is certainly acceptable.

The distance to a group of masers associated to SVS 13 in NGC 1333 has recently been obtained from multi epoch VLBI interferometry and is reported as 235±18 pc, Hirota et al. ([2008]). Chen, Launhardt and Henning ([2009]) prefer a distance 350 pc for consistency with the literature but reduction of the distance with a factor 223/350 might influence the deduction of the protostar parameters and the separation of the components of the binary protostar in SVS 13 B subcore, as discussed in Section 4.4 of Chen, Launhardt and Henning ([2009]). Knowing precise linear dimensions in a cloud is of course of some relevance for the discussion of rotational and orbital energies.

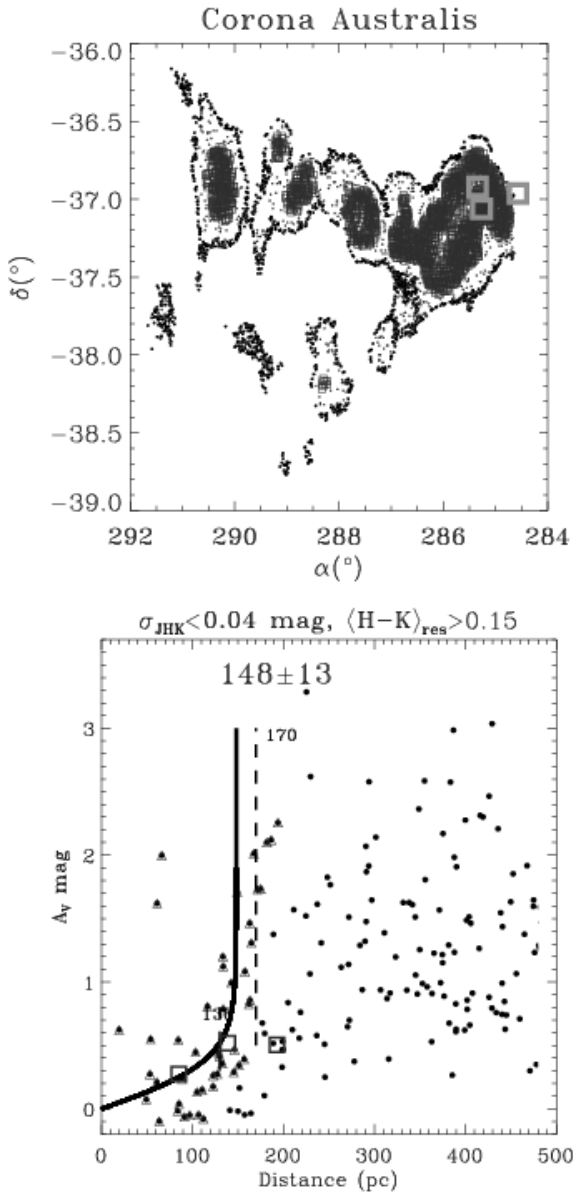

Figure 25: In the *upper frame* the Corona Australis cloud when confined by $\sigma_{JHK} < 0.040$ and $0.15 < \overline{H-K_{res}} < 0.16$. The darkest points indicate the denser reseaus with $\overline{H-K_{res}} > 0.20$. The *lower panel* shows the extinction – distance variation and the resulting estimate of the Corona Australis cloud distance D_{cloud}=148±13 pc. The dashed line at 170 pc is from Knude and Høg ([1998]). The three squares represent the three B-type Hipparcos stars used by Neuhäuser and Forbrich ([2008]) for a cloud distance 130 pc

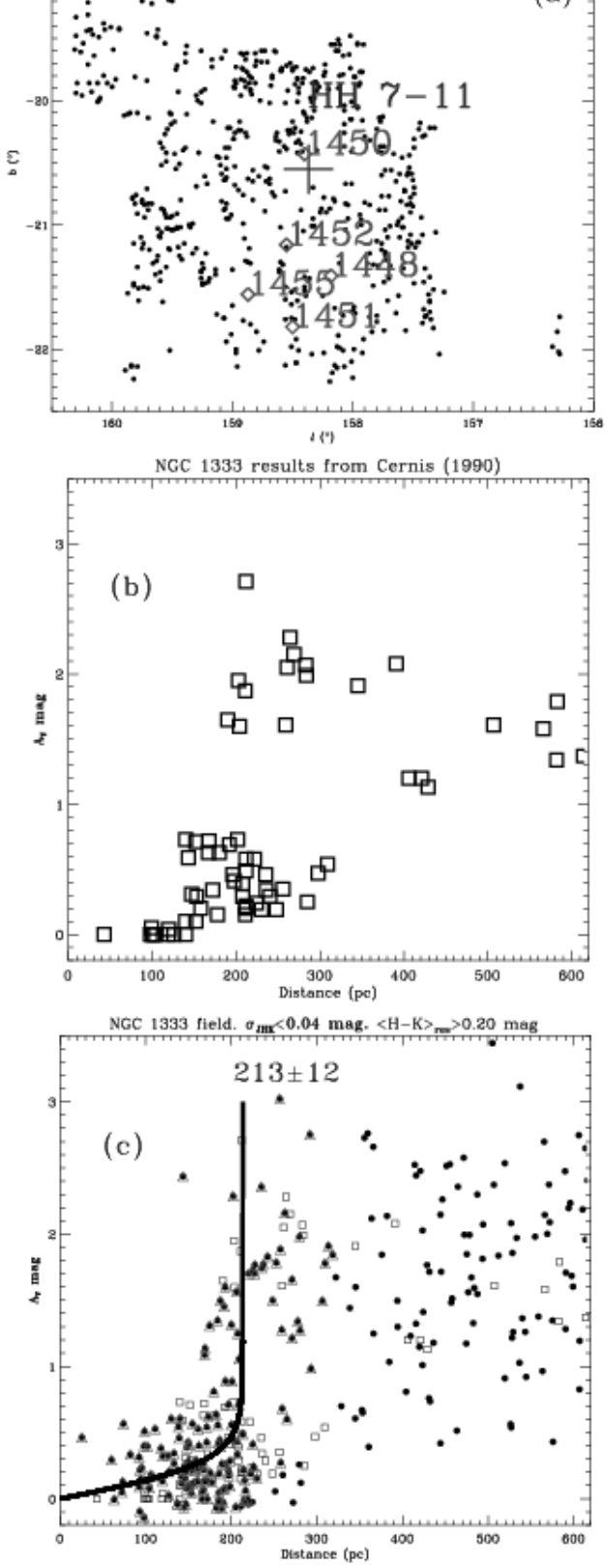

Figure 26: NGC 1333 in the Perseus complex. (a) Collection of stars with σ_{JHK} ≤0.040 mag and $\overline{H-K_{res}}$ greater than 0.20 from a 4×4 □° region centered on the NGC 1333 position (l, b) = (158.3°, -20.5°). The cross indicates HH 7-11 or SVS 13 for which an accurate parallax has been established, Hirota et al. ([2008]), D_{SVS13} = 235±18 pc. Other numbers designate dark nebulae from the Lynds catalog. (b) Resulting extinction – distance pairs from Černis ([1990]) derived from Vilnius photometry. Dust was suggested at 160 pc and at 220±20 pc from these data. (c) Extinction - distance pairs for stars in reseaus with $\overline{H-K_{res}}$ > 0.20 mag and with σ_{JHK} < 0.040 mag. The solid curve indicates the arctanh fit to the sample confined by D_{max} = 350 pc. Small triangles are the Vilnius data given for comparison

4.18 The California Molecular Cloud

The cloud containing NGC 1333 is part of the complex of clouds termed the Perseus Cloud. It has recently been realized that the sky close to the Perseus and Taurus-Auriga complexes contains a major molecular, coherent cloud, Lada, Lombardi and Alves ([2009]). The location has been known to contain a string of Lynds dark clouds. The new cloud is termed the California Molecular Cloud and with a distance 450±23 pc suggested by Lada, Lombardi and Alves it aspires to be a giant molecular complex of a $\sim 10^{+5}$ $M_\odot$ mass and a linear extent of ∼80 pc.

In their derivation of the distance 450 pc Lada, Lombardi, and Alves ([2009]) quotes previous photometric distance estimates to dust layers at distances 125 and 300 – 380 pc, Eklöf ([1959]) but suggest that these layers may not be associated with the California Molecular Cloud (CMC) but rather have their origin in Taurus-Auriga and Perseus complexes at ≈140 and ≈250 pc and thus falls short of the 450 pc.

The results from Eklöf ([1959]) are based on blue and red photographic photometry and spectral classification from Schmidt plates of 1800 stars in the Auriga region.

We estimate distances 147±10 and 213±12 pc for Taurus and Perseus respectively, see Table 2. Since CMC may rival the Orion giant molecular clouds as the most massive cloud within 0.5 kpc its distance is of interest and it is included in the present study. Fig. 27(a) shows the outlines of the cloud indicated by reseaus with $\overline{H-K_{res}} > 0.23$ and 0.28 (small ⋄s) respectively. The large diamonds of panel (a) display the location of the two strings of Lynds dark clouds and also the location of NGC 1579 (△). Panel (b) is the resulting variation of extinction with distance for the same two samples. From the $\overline{H-K_{res}} > 0.23$ mag, $\sigma_{JHK} < 0.040$ mag sample with D_{max}=500 pc from FWHM of the $A_V/D_\star$ variation. The distance of CMC becomes 330±5 pc.

A closer inspection of Fig. 27(b) reveals an apparent absence of stars between ≈200 and ≈300 pc and with A_V ranging from about 1 to about 2 so it appears that there is a cloud layer in front of the CMC proper. Assuming that this layer is connected to the Perseus cloud and not to the CMC layer we may correct for its influence on the distance estimate by removing the stars indentified in a way similar to identifying the sample used to estimate $D_{NGC\ 1333} = D_{Perseus} = 213$ pc by using $D_{max} = 350$ pc and remove these stars, supposed to belong to a Perseus layer of clouds, from the $\overline{H-K_{res}} > 0.23$ mag, $\sigma_{JHK} < 0.040$ mag D_{max}=500 pc sample. The CMC estimate is thus raised to 362±3 pc shown in Fig. 27(b) as the thin solid curve.

CMC is an example of a cloud where we may overestimate the number of M4 – T tracers because we mistake O – G6 extincted by more than 6 – 3 mag for less reddened late type dwarfs. We have therefore tried to exclude the M4 – T stars from the $\overline{H-K_{res}} > 0.23$ mag, $\sigma_{JHK} < 0.040$ mag D_{max}=500 pc sample. D_{CMC} now becomes 328±4 pc as shown in Fig. 27(c).

We suggest accordingly that D_{CMC} is between 330±5 pc and 362±3 pc or roughly 100 pc less than estimated by Lada, Lombardi, and Alves ([2009]). Interestingly this distance range is within the distance limits suggested by Eklöf ([1959]) for the second cloud layer in his Auriga survey, 300 – 380 pc. The smaller distance will cause a decrease of the linear extent to ≈60 pc and of the mass to $\sim 10^{+4.73}$ $M_\odot$.

5 Summary of distances to ∼25 local clouds

Table 2 summarizes distances to the clouds we have considered. Apart from DC300.2-16.9 where a sufficient number of stars were not available all distances and standard deviations result from the $A_{V,\ estimate} = arctanh^p(D_\star/D_{cloud})$ fitting procedure. In the Table we have indicated that the Serpens cloud was used as a template for developing our method.

6 acknowledgements

This publication makes use of data products from the Two Micron All Sky Survey, which is a joint project of the University of Massachusetts and the Infrared Processing and Analysis Center/California Institute of Tech-

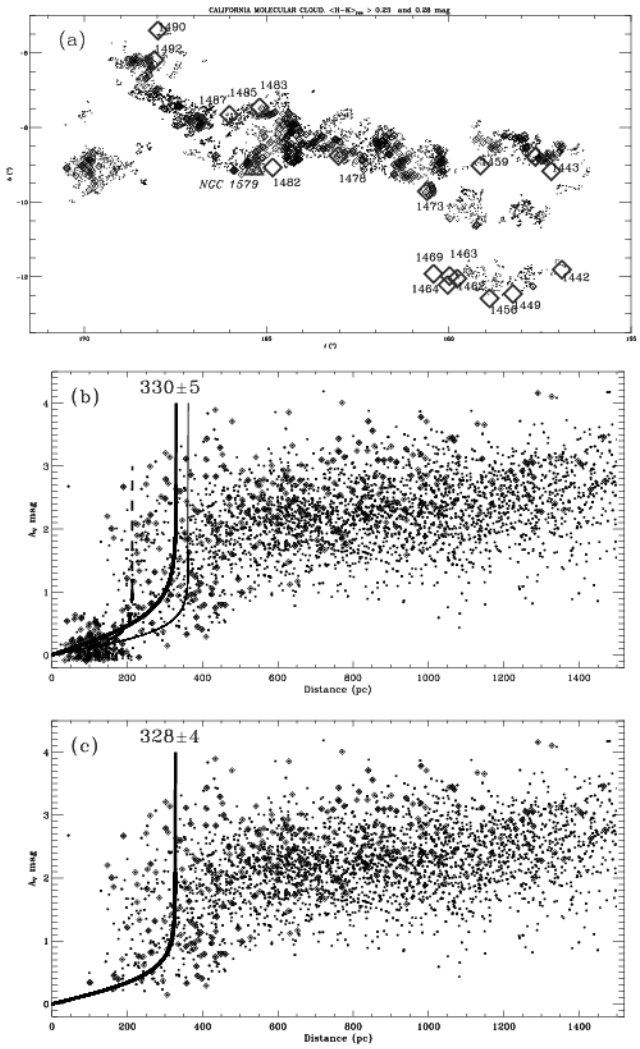

Figure 27: The California Molecular Cloud. (a) Collection of stars with σ_{JHK} ≤0.040 mag and $\overline{H-K_{res}}$ greater than 0.23. Small diamonds are stars located in reseaus with $\overline{H-K_{res}}$ greater than 0.28. Large diamonds indicate Lynds dark clouds and the triangle marks the position of NGC 1579. (b) Resulting extinction – distance pairs from the $\overline{H-K_{res}} > 0.23$ mag, $\sigma_{JHK} < 0.040$ sample. D_{max} = 500 implies D_{CMC} = 330±5 pc (thick solid curve). The dashed curve corresponds to $D_{NGC1333(Perseus)}$ = 213±12 pc, see Fig. 26. The thin solid curve, D_{CMC} = 362±3 pc, results when the *"Perseus layer stars"* with D_{max} = 350 pc are excluded from the distance estimate. (c) Extinction - distance pairs for stars in reseaus with $\overline{H-K_{res}} > 0.23$ mag and with $\sigma_{JHK} < 0.040$ mag without the M4 – T stars. The solid curve indicates D_{CMC} = 328±4 pc. Again the small diamonds show the $\overline{H-K_{res}}$ greater than 0.28

Table 2: Hipparcos/2mass distance estimates to nearby clouds

Name	D_{CLOUD} pc	$\pm \sigma_{CLOUD}$ pc
Serpens (template)	193	±13
Taurus	147	±10
Ophiuchus	133	±6
LDN 204	133	±6
LDN 1228	235	±23
LDN 1622	233	±28
LDN 1634	266	±20
Lupus I	144	±11
Lupus II	191	±13
$Lupus\ III_A$	205	±5
$Lupus\ III_B$	155	±3
$Lupus\ III_C$	230	±21
Lupus IV	162	±5
Lupus V	162	±11
Lupus VI	173	±10
Chamaeleon I	196	±13
Chamaeleon II	209	±18
Chamaeleon II	217	±12
$Chamaeleon_{I,\ II,\ III}$	194	±9
DC300.2-16.9	118::	±24
Musca	171	±18
Southern Coalsack	174	±4
Circinus	436	±29
$DC314.8\text{-}05.1_{1.jump}$	372:	±52
$DC314.8\text{-}05.1_{2.jump}$	610:	±25
$IC\ 5146_{Northern\ filament}$	603:	±68
$IC\ 5146_{cluster}$	766:	±112
Corona Australis	148	±13
LDN 1459 or NGC 1333 – part of the Perseus cloud	213	±12
California Molecular Cloud	330	±5

nology, funded by the National Aeronautics and Space Administration and the National Science Foundation. This research has made use of the SIMBAD database, operated at CDS, Strasbourg, France.

Claus Fabricius is sincerely thanked for his contributions to the early stages of this work.

References

[2000] Allen's Astrophysical Quantities, Fourth Edition, ed. Arthur N. Cox

[2006] Alves, F.O., Franco, G.A.P. 2006, MNRAS 366, 238

[2007] Alves, F.O., Franco, G.A.P. 2007, A&A 470, 570

[2004] Andersson, B.-G., Knauth, D.C., Snowden, S.L., Shelton, R.L., Wannier, P.G. 2004, ApJ 606, 341

[1999] Bally, J., Reipurth, B., Lada, C.J., Billawala, Y. 1999, AJ 117, 410

[2009] Bally, J., Walawender, J., Reipurth, B., Megeath, S.T. 2009 AJ 137, 3843

[2006] Bertout, C., Genova, F. 2006 A&A 460, 499

[1988] Bessell, M.S., Brett, J.M. 1988, PASP 100, 1134

[1999] Cambrésy, L. 1999, A&A 345, 965

[2001] Carpenter, J.M. 2001, AJ 121, 2851

[1990] Černis, K. 1990 Ap&&SS 166, 315

[2009] Chapman, N. L., Mundy, L.G. 2009, Astro-ph.GA 0905.0655v1

[2009] Chen, X., Launhardt, R., Henning, T. 2009 ApJ 691, 1729

[2008] Comerón, F., 2008, Handbook of Star Forming Regions Vol. II: The Southern Sky ASP Monographs Publications Vol.5, Edited by Bo Reipurth, p. 295

[2008] Conelly, M.S., Reipurth, B., Tokunaga, A.T. 2008 AJ 135, 2496

[2007] Cordier, D., Pietrini, A., Cassisi, S., Salaris, M. 2007, AJ 133, 468

[1997] Corradi, W.J.B., Franco, G.A.P., Knude, J. 1997, A&A 326, 1215

[2004] Corradi, W.J.B., Franco, G.A.P., Knude, J. 2004, MNRAS 347, 1065

[2002] Dahn, C.C. et al. 2002, AJ 124, 1170

[1959] Eklöf, O. 1959 Arkiv for Astronomi

[2007] Enoch, M.L., Glenn, J., Evans II, N.J., Sargent, A., I., Young, K.E., Huard, T.L. 2007, ApJ 666, 982

[2007] Flaherty, K.M. et al. 2007, ApJ 663, 1069

[1999] Fitzpatrick, E.L. 1999, PASP 111, 63

[2009] Fitzpatrick, E.L., Massa, D. 2009, ApJ 699, 1209

[2007] Harvey, P., Merín, B., Huard, T.L., Rebull, L.M., Chapman, N., Evans II, N.J., Myers, P.C. 2007, ApJ 663, 1149

[2008] Harvey, P.M., Huard, T.L., Jørgensen, J.K., et al. 2008, ApJ 680, 495

[2002] Herbig, G.H., Dahm, S.E. 2002 AJ 123, 304

[1995] Hilton, J., Lahulla, J.F. 1995 A&AS 113, 325

[2008] Hirota, T., Bushimata, T., Choi, Y.K., et al. 2008 PASJ 60, 37

[1979a] Knude, J. 1979a A & AS, 38, 407

[1979b] Knude, J., 1979b A & A, 77, 198

[1979c] Knude, J., 1979c A & A, 71, 344

[1998] Knude, J., Høg, E. 1998, A & A, 338, 897

[2001] Knude, J., Nielsen, A.S. 2001, A&A 373, 714

[2002] Knude, J., Fabricius, C., Høg, E., Makarov, V. 2002 A&A 392, 1069

[2003] Knude, J., Fabricius, C. 2003 Baltic Astron. 12, 508

[1994] Lada, C.J., Lada, E.A., Clemens, D.P., Bally, J. 1994, ApJ 429, 694

[1999] Lada, C.J., Alves, J., Lada, E.A. 1999 ApJ 512, 250

[2009] Lada, C.J., Lombardi,M., Alves, J. 2009 ApJ 703, 521

[2003] Lallement, R., Welsh, B.Y., Vergeley, J.L., Crifo, F., Sfeir, D. 2003, A&A 411, 447

[2002] Leggett, S.K. et al. 2002, ApJ 564, 452

[2008] Loinard, L., Torres R.M., Mioduszewski, A.J., Rodrígues 2008, ApJ 675, L29

[2008] Loinard, L., Torres R.M., Mioduszewski, A.J., Rodrígues 2008, RevMexAA (Serie de Conferencias) 34, 14

[2001] Lombardi, M., Alves, J. 2001, A&A 377, 1023

[2006] Lombardi, M., Alves, J., Lada, C.J. 2006, A&A 464, 781

[2008] Lombardi, M., Lada, C.J., Alves, J. 2008, A&A 489, 143

[2010] Lombardi, M., Lada, C.J., Alves, J. 2010, A&A 512, 67

[2008] Luhman, K.L. 2008, Handbook of Star Forming Regions Vol. II: The Southern Sky ASP Monographs Publications Vol.5, Edited by Bo Reipurth, p. 169

[2008] Luhman, K.L., Muench, A.A. 2008, ApJ 684, 654

[2008] Luhman, K.L, Allen, L.E., Allen, P.R., Gutermuth, R.A., Hartman, L., Mamajek, E.E., Megeath, S.T., Myers, P.C., Fazio, G.G. 2008 ApJ 675, 1375

[2007] Makarov, V.V. 2007, ApJ 658, 480

[2007] McKee, C.F., Ostriker, E.C. 2007, Ann.Rev.Astron.Astrophys. 45, 565

[2008] Merín, B., Jørgensen, J., Spezzi, L., Alcalá, J.M., Evans II, N.J., Harvey, P.M., Chapman, N.,Huard, T., van Dishoeck, E.F., Comerón, F. 2008 arXix: 0803.1504v1

[1997] Meyer, M.R., Calvet, N., Hillenbrand, L.A. 1997, ApJ 114, 288

[1994] Mikami, T., Ogura, K. 1994, MNRAS 270, 199

[1952] Münch, G., 1952, ApJ 116, 575

[2008] Neuhäuser, R., Forbrich, J. 2008, Handbook of Star Forming Regions Vol. II: The Southern Sky ASP Monographs Publications Vol.5, Edited by Bo Reipurth, p. 735

[1980] Neckel, Th., Klare, G. 1980, A&AS 42, 251

[2008] Nehmé, C., Gry, C., Boulanger, F., Le Bourlot, J., Pineau des Forês, Falgarone, E. 2008, A&A 483, 471

[1997] Padoan, P., Jones, B.J.T., Nordlund, Å 1997, ApJ 474, 730

[1997] Perryman, M.A.C., Lindegren, L., Kovalewsky, J., Høg, E., Bastian, U., et al. 1997, A&A 323, L49

[2007] Porras, A., Jørgensen, J.K., Allen, L.E., et al 2007, ApJ 636, 493

[2002] Reid I.N. , Cruz K.L 2002, AJ 12 2806

[2008] Reipurth, B., Megeath, S.T., Bally, J., Walawender, J. 2008, Handbook of Star Forming Regions Vol. I: The Northern Sky ASP Monographs Publications Vol.4, Edited by Bo Reipurth, p. 782

[1985] Rieke, G.H., & Lebofsky, M.J. 1985, ApJ 288, 618

[2008] Snow, T.P., Destree, J.D., Welty, D.E. 2008, ApJ 679, 512

[1996] Straižys, V., Černis, K., Bartasiute, S. 1996 Baltic Astron. 5, 125

[2001] Tachihara, K., Toyoda, S., Onishi, T., Mizuno, A., Fukui, Y., Neuhäuser, R. 2001 PASJ 53, 1081

[2005] Teixeira, P.S., Lada, C.J., Alves, J.F. 2005 ApJ 629, 276

[2007] Torres, R.M. Loinard, L., Mioduszewski, A.J., Rodríquez 2007, arXiv:0708.4403v1 [astro-ph]

[1997] Whittet, D.C.B., Prusti, T., Franco, G.A.P., et al. 1997, A & A 327, 1194

[2007] Whittet, D.C.B., 2007, AJ 133, 622

[2009] Winston, E., Megeath, S.T., Wolk, S.J. et al. 2009 astro-ph 0904.1244v2

A The $(J-K)_0 - M_J$ calibration of the main sequence

A.1 The calibration sample

To have intrinsic colors we are obliged to use nearby, presumably unreddened, stars from the Hipparcos Cataloque, Perryman et al. ([1997]). To obtain a precise calibration we use stars with $\pi \geq 0.010$", assumed to imply virtually no reddening, and with a relative error better than 10%. The stars fulfilling these two criteria constitute the astrometric sample. The astrometric sample is compared to the 2mass catalog and the common stars are extracted.

For several entries the Hipparcos Catalogue contains spectral and luminosity classification from the literature. A substantial part of the stars common to 2mass and Hipparcos does, however, not have any classification but may anyway be dwarfs and should be included in the sample in order to substantiate the main sequence calibration. Fig. 28 shows the distribution of the stars without classification (gray points) overplotted the astrometric sample (black points). More than 5500 stars meeting the $\pi \geq 0.010$" and $\sigma_\pi/\pi \leq 10.0\%$ criteria are without a luminosity classification.

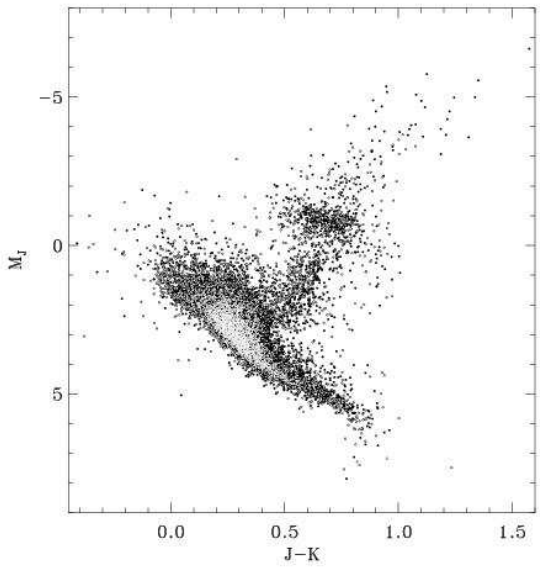

Figure 28: Dark points all Hipparcos stars fulfilling the astrometric criteria: $\pi \geq 0.010$" and $\sigma_\pi/\pi \leq 10.0\%$. The overplotted lighter points are those without luminosity classification and many of these must be main sequence stars and should accordingly be included in the calibration sample

A.2 Confining the main sequence

Some stars classified as evolved are better appreciated as main sequence stars. There is a concentration of stars classified as LC IV as well as LC III at $(J-K,\ M_J) \approx (\ 0.2,\ +2)$. A possible reason for classifying stars in the color range from about 0.1 to 0.3, the approximate A6 – F5 region, as "giant" like could be that they have a small Vsini for their color? To have as many precise main sequence stars as possible for the color – absolute magnitude calibration we do not rely entirely on the luminosity classification given in the Hipparcos Catalogue but try to delineate what we think is the proper main sequence.

It is important to separate the main sequence from the subgiant branch: the region around $(J-K, M_J) \approx (0.5, 3.0)$ where the MS and giant branch are separated by ∼3 mag in M_J. A mean or median value of M_J at $(J-K)$ ≈0.5 would be located in the gap and would represent no stars. Stars in the Hipparcos/2mass cut are included in the calibration sample if located inside the main sequence demarcation as defined in the following (result in Fig. 31). Apart from the apparent confinement in the $(J-K)_0$ *vs.* M_J plane we corroborate "our main sequence" in two ways. It turns out that the J, H, and K bands are not equally sensitive to evolution so we use the branching in the M_J *vs.* M_K diagram, Fig. 29, for a coarse separation of giants from dwarfs. And we use theoretical isochrones to help confining the main sequence to the blue and to the bright, evolved side.

The resulting confinement is shown in Fig. 31. The issue for introducing this confinement is to obtain a separation of LC V and IV in the turn off region. The M_J *vs.* M_K diagram is useful by suggesting a separation of the giant and dwarf sequences. In Fig. 29 is shown how the M_J and M_K magnitudes separate in the M_J range from +3 to -2 in a giant and a dwarf branch. For any given M_J magnitude in this range the giants are more luminous in the K band than the dwarfs. For a distinction between the two luminosity classes we fitted an upper envelope to the dwarfs in the form of a straight line to the brightest part of the main sequence. According to Fig. 28 the partition is to run in the $(J-K)$ range from about 0.3 to about 0.45. The lower K-luminosity limit for the giants is suggested as: $M_K \approx 0.97575 \times M_J - 0.33265$. The solid line is the proposed division between giants and dwarfs, the dashed line is a 45° line.

When the dividing line is transformed to the $(J-K) - M_J$ plane it defines the partition between class V and class IV. The division is shown in Fig. 30.

Stars classified as LC IV in the Hipparcos/2mass sample are overplotted as light gray points circles in

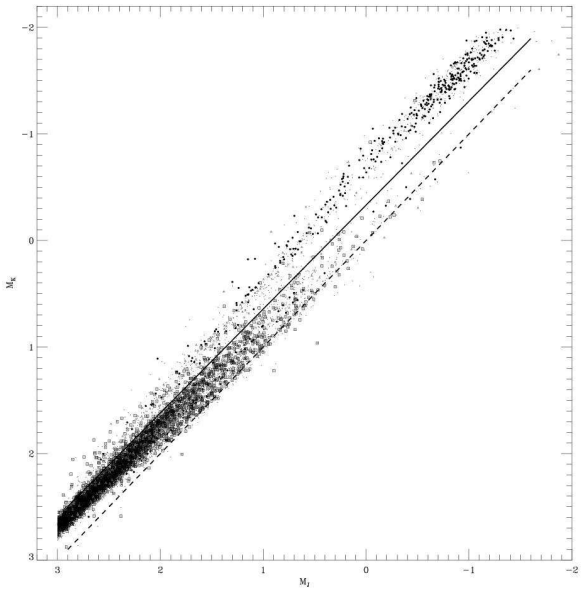

Figure 29: The branching part of the M_J *vs.* M_K diagram which is used for separating LC V (tiny boxes) from LC III (black points) and from LC IV (triangles). The upper solid curve is the line dividing dwarfs and giants and the lower dashed curve is a 45° line.

Fig. 30 and we notice that there is a clear coincidence of the transformed dividing line from Fig. 29 and the upturn of the subgiants indicated by a set of isochrones on Fig. 30.

Another important issue is how the upper luminosity limit of the early part of the main sequence should be identified? Important because of its influence on the spread assigned to the estimated absolute magnitudes. Fig. 28 shows how sparsely populated it is in the Hipparcos sample. The upper confinement for this part of the main sequence might instead be based on all stars from the 2mass/Hipparcos comparison, irrespective of parallax and its relative error. In this sample even the blue $(J-K)$ limitation, which seems virtually uninfluenced by extinction is well defined. The upper bright limit is, however, drawn where the brightest members in the astrometric sample are located (see Fig. 28 and Fig. 30) and not at a virtually constant $M_J \approx +1$ where the bulk of the calibration sample has its bright limit.

Theoretical isochrones in the infrared, *JHK*, have been published by Cordier et al. ([2007]) and the Hipparcos/2mass main sequence stars should be confined by a very young and moderately old isochrones. The very young one should coincide with the youngest stars in the sample and delineate the lower luminosity boundary together with the blue main sequence confinement. The moderately old ones, younger than a few Gyr, might help locate where A type stars and earlier types leave the main sequence. We have included a set of such isochrones in Fig. 30 with ages ranging from 0.1 to 8.0 Gyr. The 0.1 Gyr isochrone is a rather good representation of the lower envelope and the blue confinement. The upper confinement of the data is located roughly where hydrogen burning in a thick shell is replaced by shell hydrogen burning. The 8 Gyr isochrone also represents the dwarf - subgiant transition rather well. Shifting to the 12.0 Gyr isochrone does not shift this red limitation significantly. In the region $(J-K) \gtrsim 0.4$ the isochrones follow a central location in the MS distribution.

Guided by these considerations we have drawn the border line around the sample. Stars inside this curve are now considered as *the* main sequence sample, and will be used for the $M_{JHK} - color$ calibrations. It is shown in Fig. 31 together with the isochrones. The precise location of the upper luminosity confinement is not that critical, except where the giants branch off. This is because the luminosity distribution across the main sequence at a given color has very few stars at the extreme luminosity. Stars at the upper main sequence confinement evolve fast implying a low density of data points and they are located at the blue limit of the Hertzsprung gap.

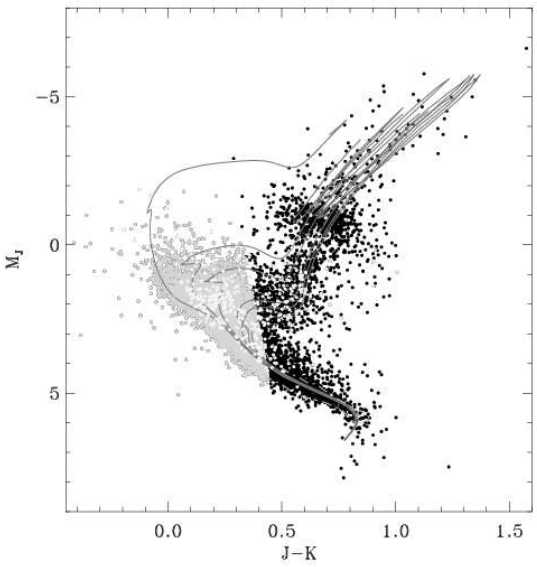

Figure 30: The figure shows the early main sequence resulting from the simple dividing line in Fig. 29. The cool part of the main.sequence is not included this way because the M_J *vs.* M_K distribution turns back to the high K-luminosity side of the dividing line. Luminosity class IV stars are overplotted as the brightest points. Isochrones of ages 0.1, 0.8, 1.5, 4.0, 5.0 and 8.0 Gyr are from Cordier et al. ([2007])

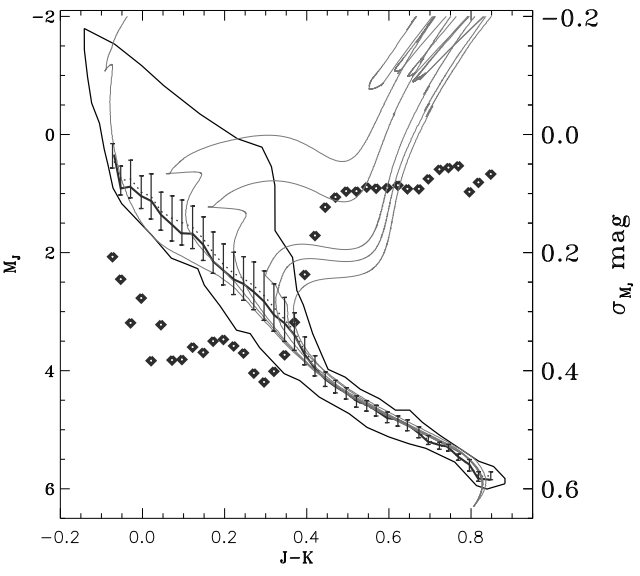

Figure 31: The thin solid curve is the confinement of the main sequence sample discussed in the text and is shown together with its resulting statistical relations calculated for 0.025 mag bins of $(J-K)$. The dotted curve is the mean given together with the standard deviation computed for 0.050 $(J-K)$ intervals. The median curve is the solid thick one. Isochrones from Cordier et al. ([2007]) are shown for 0.1, 0.8, 1.5, 4.0, 5.0 and 8.0 Gyr. The diamonds show σ_{M_J} (right hand scale) calculated for overlapping 0.050 intervals in $(J-K)$ separated by 0.025 mag and a drop from 0.4 mag to 0.1 mag is noted where the 8 Gyr isochrone turns off the main sequence

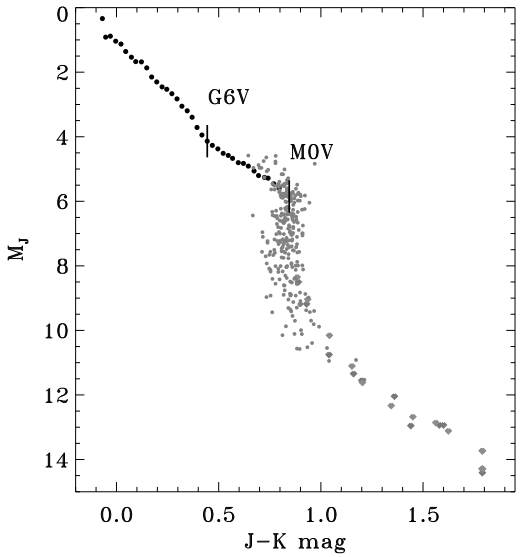

Figure 32: For illustration we show the complete main sequence including M and L dwarfs. Early main sequence, black points, is from the present work. Grayish points are M dwarfs from Reid and Cruz ([2002]) and the cool tail of L dwarfs are from Leggett et al. ([2002]) and Dahn et al. ([2002]). For the L dwarfs both median and mean values are displayed

A.3 Mean and Median Loci

The sample within the main sequence confinement and meeting $\pi \geq$10 mas and $\sigma_\pi/\pi \leq$0.10 criteria consists of 9085 stars. Since it is not possible to give a precise location of a star in the $(J-K)_0$ *vs.* M_J diagram from only three photometric bands we replace the main sequence with a locus giving a representative absolute magnitude as a function of a color. Due to the natural width of the main sequence the replacement will introduce offsets from the true magnitude.

A.3.1 Mean Locus

After dividing the main sequence into 0.025 mag intervals in $(J-K)_0$ we compute the mean and standard deviation of the color and the absolute magnitude for each color bin. The run of the mean locus is given as the dotted curve in Fig. 31. The standard deviation is calculated for 0.050 $(J-K)_0$ bins though but are plotted for every 0.025 mag intervals. The standard deviation represents the error we commit by using the mean main sequence locus. The standard deviation is plotted as diamonds referring to the right hand scale of the figure. There is a dramatic decrease in the σ_{M_J} values with a factor $\gtrsim$2 in the $(J-K)$ bin 0.3 – 0.5 from $\approx$0.4 to $\approx$0.1. The errors range from $\approx$0.06 to $\approx$0.4 for the late and early types respectively. Paying no attention to any other error source the inaccuracy translates to a relative distance error $\Delta R/R$ ranging from 3% to 20% for individual stars with $\sigma_{J,K}$ <0.035 mag. The inaccuracy will apply to the estimate of *individual* stellar distances. The features whose distances interest us − extinction discontinuities − are defined by several stars, maybe a number $\gtrsim$10 implying an error of the mean distance better than $\gtrsim$10%. The sequence of errors narrows at about $(J-K)_0 \approx$0.45 corresponding to early G dwarfs. The red termination of the sequence is at K7 – M0. M dwarfs are thus not included in this calibration but dedicated studies of their infrared absolute magnitudes have become avaible in the literature, Dahn et al. ([2002]), Leggett et al. ([2002]), Reid and Cruz ([2002]). Fig. 32 shows how the absolute magnitudes of the M and L dwarfs fit into the present calibration. From the error point of view late G and K dwarfs are very well suited for the distance derivation but as seen in Appendix B on the *JHK* data these stars may not be of immediate use due to the giant-dwarf degeneracy and the shape of the main sequence in the two color $(H-K)$ − $(J-H)$ diagram. In Sect. B.3 and B.4 we suggest how these stars possibly may be

included in the distance derivation.

A.3.2 Median Locus

With the same color binning as for the mean we calculate the median color and absolute magnitude for each bin. The solid black curve of Fig. 31 shows the resulting median curve and for the early part of the diagram we notice that the median locus is slightly fainter than the mean which was to be expected.

A.4 Dispersion in the distance calibration

As a test we have applied the median calibration on the calibration sample itself following the prescription of Subsection 3.3. Only for spectral types earlier than ~G6V though, by running the sequence of codes used for the distance and extinction estimates we have developed for the 2mass data. Note that this spectral range has the most imprecise calibration with $\sigma_{M_J} \approx 0.4$ mag.

For this excersize we can not assume that the Hipparcos sample is unreddened but must estimate the intrinsic colors, $(H-K)_0$ and $(J-H)_0$, as we do with any 2mass extraction. We have no demands to the accuracy of the JHK photometry. From the $(J-K)_0$ vs. M_J calibration we have the distance estimate which we compare to the trigonometric distance π^{-1}. The mean difference of these distances becomes 8.8 pc and the standard deviation about 25 pc. The dispersion of the mean differences is $\lesssim$10 pc and derives almost exclusively from the astrometric errors. Since the mean difference only differs from zero on the sigma level we have not decreased the calibrated distances with the zero point offset. If we subtract the error coming from the trigonometry the dispersion of the distribution of residuals decreases to $\approx$20 pc. All stars being closer than 100 pc this dispersion agrees with our calculated standard deviations of M_J in the range from 0.2 to 0.4. 0.4 is the value pertaining to stars earlier than G6V. σ_{M_J}=0.4 implies a relative uncertainty in a single distance of 18%.

B The JHK data

Knude and Fabricius ([2003]) presented a preliminary discussion of the Hipparcos/2mass combination applied to distances of interstellar features. For the JHK extraction an oversized area in the direction under investigation is defined and the errors and flags to be accepted are selected. For clouds in the solar vicinity outlines are known from mm observations of ^{12}CO rotational lines or from optical or infrared extinction maps. If not available the complete set of *JHK* observations itself offers an estimate of the outline either from simple star counts or from contours of mean values of $(H-K)$ formed in a reseau centered on each extracted 2mass star.

It has proven to be of some importance leaving out the photometry with the largest errors for the distance and extinction derivation whereas the complete sample is retained for the star counts. Most often we base $\overline{H-K}_{res}$ contours on stars with precise photometry $\sigma_{JHK} \leq 0.04$ but the limit is sometimes relaxed to 0.06 or even to 0.08 to include a larger number of stars.

Star counts are done in circular reseaus required to contain 100 counts on the average. A count is assigned to each entry in the extraction from the 2mass catalog thus leaving out a margin the size of the radius of the reseau of the originally defined area on the sky. The reseau radius is typically $\lesssim 10'$. The reseau size depends on the galactic latitude ranging from ~15′ at the poles to ~5′ close to the plane. Even a change of a few degrees in latitude may change the appearence of a cloud as given by counts. Neighboring counts are thus not independent but the stars outlining a given count is only used for indicating the possible presence of extinction and not for evaluating its size or extinction.

Fig. 33 and 34 both cover two dense knots of Lupus IV located approxmately (α, δ) =(242.8, -41.7) and (242.1, -41.7). See e.g. Fig. 8 of Cambrésy or the CO map in Fig. 2 of Tachihara et al. ([2001]) or the more recent extinction map by Lombardi, Lada and Alves ([2008]). See also the $\overline{H-K}_{res}$ map in Fig. 13. The scales of the two Figures are identical so the suggested dimensions of the knots are quite different when counts less than 125/reseau is used as the defining limit and they are not reproduced in the $\overline{H-K}_{res}$map of the same region, Fig. 13. The low declination field, Fig. 34, suggests a size four to five times larger than the high declination

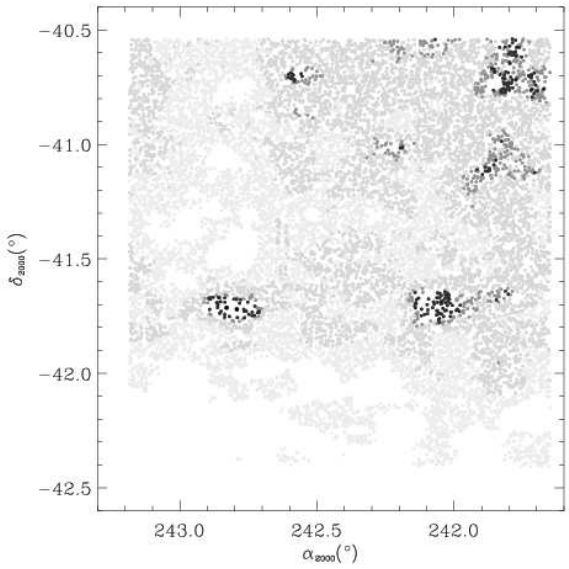

Figure 33: Region containing eastern part of the Lupus IV cloud. Reseaus displayed are those with less than 150, 125, 100 and 90 stars/reseau respectively. Very few stars are located in reseaus with less than 75 stars/reseau (large black dots)

field, Fig. 33. This tendency may be understood as an effect of the galactic latitude. Increasing the latitude will lower the average stellar density, and increase the reseau size required to contain 100 stars on the average. There is no unique *apriori* way to define the area from which stars may be drawn for the distance determination of the cloud. Extinction contours drawn from mean $H-K$ reseau values may likewise be influenced by latitude because the stellar distribution varies with latitude. A cloud confinement is defined by a lower $\overline{H-K}_{res}$ limit identified just outside the cloud perimeter, see Fig. 7(b).

B.1 Which parts of the $(H-K)$ − $(J-H)$ diagram may be used for the intrinsic color estimate? The Serpens region as an example

In Fig. 35 we have shown the color magnitude diagram $(J-K)$ vs. J for a 2×2 □° box confining part of the Serpens molecular cloud and overlaid with a set of isochrones from Cordier et al. ([2007]) for comparison. The isochrones are shifted 10.5 mag and assuming reddening of E_{J-K} = 0.6. The 10.5 mag is chosen because with this shift a few giants are located on the 8 – 12 Gyr isochrone and we note that the shifted 8 and 12 Gyr isochrones and the upper confinement of the shifted main sequence almost are superposed in the $(J-K)$ vs. J diagram for $(J-K) \gtrsim 1.0$. A main sequence may be identified as well as a very broad giant branch where the width probably is caused by extinction.

The black points of Fig. 37 show the $(H-K)$ vs. $(J-H)$ two color diagram for the same stars. The main sequence and giant relations from Bessell and Brett ([1988]) supplemented with the relations from Dahn et al. ([2002]) and Leggett et al. ([2002]) for the cool dwarfs and from Allen ([2000]) for the hot stars not contained in Bessell and Brett are overplotted. The relations have been transformed to the 2mass system, Carpenter ([2001]).

Two straight lines with the slope of the reddening ratio E_{J-H}/E_{H-K}=1.916 assumed to be constant for all spectral classes are shown. The value, 1.916, is close to the ratio derived from Fitzpatrick's ([1999]) model of the extinction law computed for R_V=3.1 and assuming a reddening E_{B-V}=0.5. This means that we use a law pertaining to the diffuse part of the interstellar medium.

The upper one of the two reddening vectors in Fig. 37 intersects the main sequence where the giant sequence has it hottest point. The lower one crosses the main sequence at its hottest point and acts as a lower envelope in

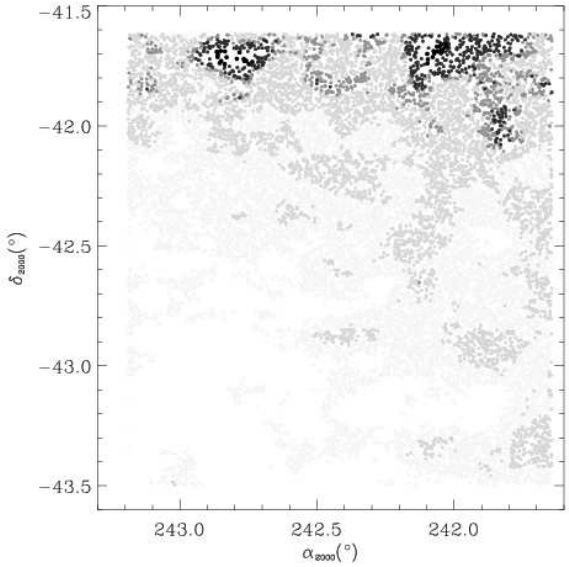

Figure 34: Region containing eastern part of the Lupus IV. Like the previous figure but shifted one degree towards the South Celestial Pole. Note that after the shift in declination more stars are located in reseaus with less than 75 stars/reseau (large black dots) and the associated dense clumps appear larger than in Fig. 33. $\overline{H-K}_{res}$ contours for this part of Lupus IV may be seen in Fig. 13

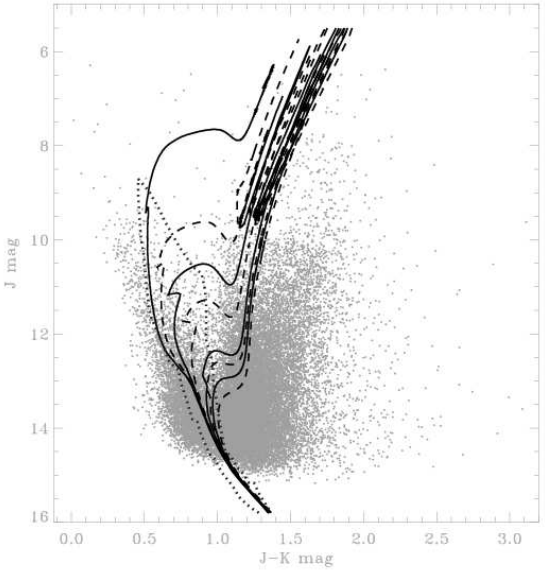

Figure 35: 2mass data from a 2×2 □° box in the direction of the Serpens star forming cloud. $(\alpha,\delta)_{center,2000}$ = $(18^h24^m, 0°0\prime)$. Slightly off set from the dense knots shown in Fig. 36. 25570 point sources with $\sigma_{JHK} \leq 0.040$. The main sequence confinement in $(J-K)-M_J$ are shown together with the 0.1, 0.4, 0.8, 1.5, 8.0 and 12 Gyr isochrones shifted 10.5 mag in J and 0.6 in $J-K$

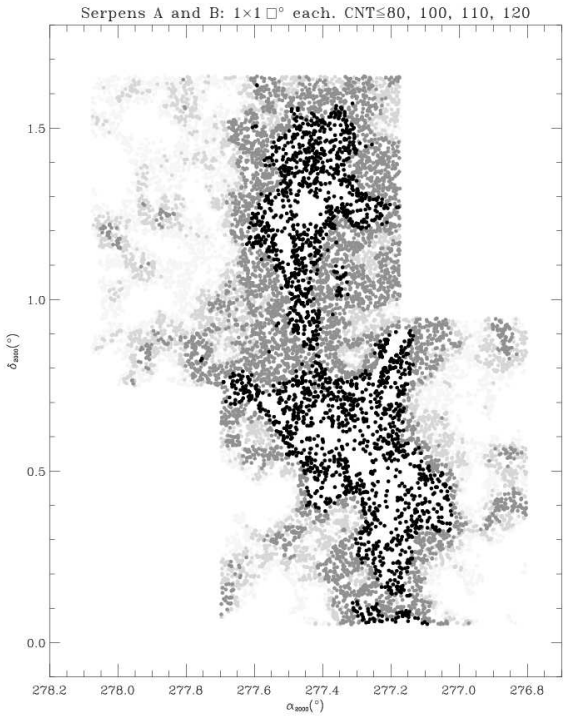

Figure 36: 2mass data for two slightly overlapping 1×1 □° regions in the direction of the Serpens star forming clouds A and B. Reseaus with counts less than 80, 100, 110 and 120 are shown. The countours of these counts may be compared to the extinction map given by Enoch et al. ([2007]) in their Fig. 5.

the color – color diagram.

To obtain intrinsic colors a main sequence star is translated parallel to a reddening vector to the standard locus with a shift given by its reddening. When a star is extrapolated back to its location on the main sequence locus its intrinsic colors $(H-K)_0$ and $(J-H)_0$ are known. This implies that we have an estimate of the star's reddening in $(H-K)$ as well as in $(J-H)$. We prefer using E_{J-H} which, apart from the larger range of $(J-H)_0$ compared to $(H-K)_0$, is relatively less influenced by the photometric errors than E_{H-K}. From E_{J-H} and the extinction law A_J is obtained. Applying the absolute magnitude calibration of the main sequence locus from in Appendix A, Fig. 31 supplemented with literature values for spectral types earlier than ∼B4 and later than ∼M0 we may estimate the stellar distance and produce a diagram showing the extinction variation with distance.

Complications arise because the giant and main sequence relations overlap and because the main sequence has the shape it has, after an almost linear dependence of $(J-K)_0$ on $(H-K)_0$ the relation breaks and $(J-H)_0$ becomes almost constant with increasing $(H-K)_0$ implying that we may not discern a heavily reddened early main sequence star from a less reddened late type main sequence stars. A degeneracy that will be remedied in the next decade when trigonometric parallaxes become available for most of the 2mass stars.

B.2 The early types on the MS

To avoid the mismatch of giants and dwarfs only stars below the upper reddening vector of Fig. 37 should be applied. And to avoid the early/late type dwarf mixing we should limit the study to reddenings pertaining to the early dwarfs located between the two parts of the main sequence locus. This implies a bias in the reddening range that may be probed. The hottest part of the main sequence may trace reddenings equivalent to $A_V \lesssim 6$ mag whereas the dwarfs located just where the giant relation branches off only measure $A_V \lesssim 3$ mag but these values are sufficient to identify an extinction discontinuity. We impose a mininum distance measured along a reddening vector from the cool part of the relation in order to assure that a point is not caused by the error distribution among the late M dwarf. Similarly we introduce a minimum distance in $(J-H)$ from the upper reddening line. We also exclude stars located to the blue side of the main sequence in terms of the $(H-K)$ color. The sample located between the two reddening vectors of Fig. 37 and confined by the main sequence locus and reduced by the imposed margins is our prime tracers of reddening and distance. These stars do,

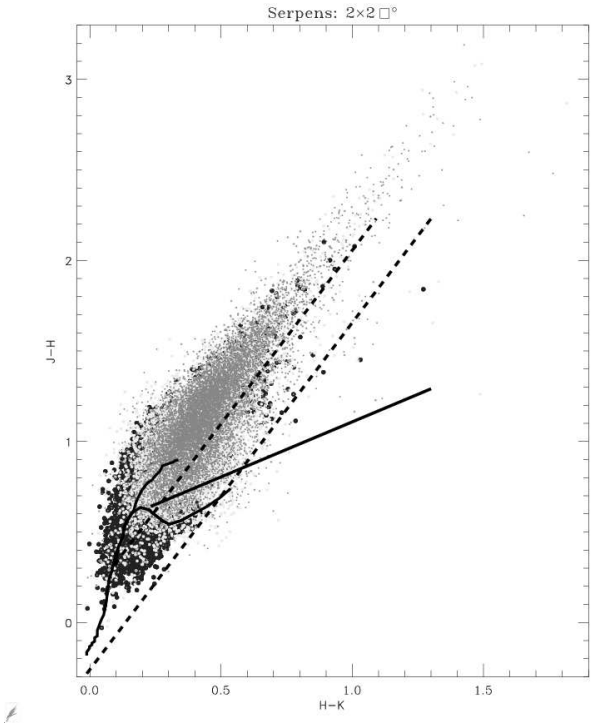

Figure 37: 2mass data from the two 1×1 □° boxes shown in Fig. 36 in the direction of the Serpens star forming clouds: A(light gray) and B(dark gray). The main sequence and giant loci are displayed together with two reddening vectors. The upper one intersects the main sequence relation where the giant relation has its origin. The third line is Meyer et al.'s ([1997]) unreddened T Tauri locus. The two cloud regions are overplotted data from the nearby 2×2 □° region shown in Fig. 35 (black symbols) covering the southern part of Fig. 36. We notice that part of the 2×2 □° region are much less reddened than the two 1×1 □° boxes

however, belong to the less populated bright part of the luminosity function with a rather low spatial density. They may trace rather large volumes and measure substantial extinction values but for nearby, small molecular clouds typically with solid angles smaller than a few square degrees, the probability to find such stars in front of the cloud is small. And for a good estimate of a cloud distance unreddened stars in front and reddened stars just behind the cloud are required. Stars with a larger spatial density may be required to trace the volume in front of any cloud. Experiments on most of the local star forming clouds have shown that the O – G6 MS range most often do not provide enough stars in front of the extinction jump. This means that the cooler K and M dwarfs should be considered in order to provide an estimate of a lower distance estimate to the cloud.

B.3 The cool dwarfs

Due to the scarcity of the early type dwarfs, few are expected in the volume in front of a cloud implying that only upper distance limits can be provided for most local molecular clouds. We therefore may try to include the M dwarfs as well. Intrinsic color and absolute magnitude are derived as for the early type dwarfs, the only difference is that we have replaced the independent parametera $(H-K)$ with $(J-H)$ because of the near $(J-H)_0$-constancy of these cool stars. We thus include stars with $(J-H)$ located above the main sequence value reduced by $\Delta(J-H) = 0.070$ for a given $(H-K)$ value and 0.040 mag below the upper reddening vector in Fig. 37. Stars below the main sequence by more than $\Delta(J-H) = 0.070$ are included in the sample of main sequence stars earlier than G6V. The chosen limitations depend on the maximum photometric errors. As a reference we use $\sigma_{JHK,max} = 0.040$ mag.

Since the volume of the molecular cloud, in the solid angle we study – which often is only a few square degrees – typically is small, the volume in front of the cloud may be used as an approximation to this volume plus the cloud volume and we may compare the number of early dwarfs (hotter than ∼G6) to the number of late dwarfs (cooler than K9/M0) from the local luminosity function. The late/early ratio becomes ≈8. Noting that the early ones that are mistaken for late ones are the ones that have their A_V exceeding the range from 3 to

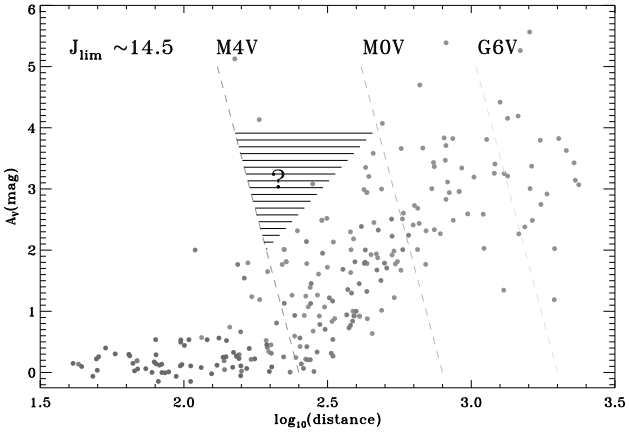

Figure 38: Extinction vs. distance data combined for the two regions Serpens cloud A and B shown in Figs. 36 and 37. The three dashed lines show the maximum extinction observable for three divisions in the $(H-K)-(J-H)$ diagram. The central line is caused by the turn over of the $(H-K)-(J-H)$ relation at the maximum main sequence $(J-H)$ value roughly corresponding to M0V. The right most corresponds to the spectral type where the the giant locus and the main sequence coincide, approximately at G6V, and finally the left most displays the maximum extinction measurable with main sequence tracers of type M4V. The upper extinction limits are valid for a limiting magnitude $J_{lim} \sim 14.5$. The hatched triangle may only be measured with stars earlier than ~M4V, see discussion in the text

about 6 mag and are emerged in the cloud with a volume that is much smaller than the volume in front of the cloud or are located behind the cloud so the late/early ratio is in fact larger than 8. The stars clustering around the lower reddening vector of Fig. 37 illustrate that contamination of the cool sample by very extincted early type stars, $A_V \lesssim 15$ mag, takes place. Another interpretation is that these are not early dwarfs but rather on the AGB, Lombardi, Lada and Alves ([2010]).

Since some molecular clouds are star forming, another, less serious ambiguity arises from the presence of PMS stars. Stars with $(J-H)$ redder than indicated by the T Tau locus given by Meyer, Calvet and Hillenbrand ([1997]) are consequently excluded. So only the stars located between the locus defined by the main sequence relation corrected with $\Delta(J-H) = 0.070$ and the T Tau line is considered for the distance – extinction determination. This of course biases the M dwarfs included in the sample to the lesser reddened ones. A nice example showing some very local unreddened M dwarf candidates for a Serpens region is shown in Fig. 38. We call these secondary tracers the M4 - T sample.

The two samples we have considered so far are firstly the one constituted by the stars confined by the main sequence and the two reddening vectors originating where the giant relation branches off the main sequence and where the hottest star included in the main sequence relation are located: this is our primary sample for which we may estimate extinction and distance in a unique way. Secondly we include the dwarfs later than ~M4 and confined by the main sequence offset by -0.070 in $(J-H)$ and by the T Tau sequence. This sample may not be clean since it may be contaminated by dwarfs earlier than ~G6 and with an extinction exceeding $\approx 3-6$ mag in V depending on the spectral class. The contamination may not bias the results seriously since assuming that all stars are ~M dwarfs only will imply a wrong type in a few cases, about one out of eight. Mistaking an O – G6 dwarf for an M dwarf will in fact not influence the location of the extinction discontinuity, e.g. the one in Fig. 38, it will replace a large extinction (the true one) with a small (a false one) but put it at a false small distance, due to the intrinsic faintness of the *M* dwarfs (Fig. 32), where it will not influence the estimate of the cloud distance seriously.

B.4 Indications from the K dwarfs

Leaving out a spectral range in a magnitude limited sample, as 2mass, may introduce selection effects influencing the distance – extinction variation we are looking for. Furthermore the G6 – MO dwarfs have a high spatial density and if they could be included in the distance – extinction determination they would substantiate the presence of any extinction discontinuity suggested by the O – G6V and M4 – T samples. Not to mentioned that G6 – M0 range has a more precose calibration than the O – G6 range.

As we can see from the $(J-K)_0$ vs. M_J relations in Fig. 32 there is a homogeneous variation of M_J with $(J-K)_0$ also in the spectral range from G6 to M0. This means that the exclusion of the ~G6 – M0 part of the main sequence will introduce a gap in the distance distribution of the extinction tracers because stars with M_J between 4 and 6 are systematically missing. There may, however, be a way that the K dwarfs can be used to corroborate the distance – extinction indications suggested by the early and the late steller types: If the distance vs. A_V diagram based on stars earlier than ~G6 and later than ~M4 indicates a well defined extinction discontinuity, refer to Fig. 38 and 19 where we notice the dwarfs later than ~M4 within ~200 pc and the O – G6 dwarfs beyond ~200 pc, we have an indication of the distance range over which the extinctions in the jump are measured.

In order to make use of the ~G6 – M0 dwarfs we first extract the stars between the upper reddening line and the main sequence, see Fig. 37. This extraction is of course a mixture of dwarfs and giants. If on the main sequence they are of spectral types ~G6 – ~M0.

With the distance – extinction information deduced from the O – G6 and M4 – T samples we have an indication of how extinction varies with distance. We know part of the extinction range within a given distance interval. In Fig. 39 we see that A_V is increasing from ≈0.3 to ≈3.5 mag within the distance interval from ~60 pc to ~450 pc. Given the A_V and distance limitations we ask if any of the stars we just extracted between the upper reddening vector and the main sequence can be located in this distance interval (60 – 450 in our example) and with an extinction in the range suggested by the M4 – T and O – G6 dwarfs respectively. Assuming they are dwarfs, i.e. that they obey the $(J-K)_0 - M_J$ calibration valid for the G6V – M0V stars, we extrapolate back to the main sequence standard curve and obtain an estimate of the intrinsic colors and subsequently absolute magnitude just as was done for the O – G6 range. Extinctions estimated for the K dwarfs this way are limited to the range from ~0 to ~3. The spatial density of the ~K dwarfs are approximately the same as that of the early group. By imposing the distance and extinction limits in the extraction of possible K dwarfs we may exclude the giants. The $(J-H)$ color range of these stars include the G0III – K2/3III spectral range for the giants implying that the ratio of the number densities of the G6V – M0V to the number density G0III – K2/3III stars is ≈36.5. The LC III stars are of course brighter than LC V stars, for $(J-K)$ ≈0.7 the red clump giants are ≈ six magnitudes brighter than the corresponding point on the main sequence. This means that since the observed J magnitude does not depend on whether the target is a dwarf or a giant, since the extinctions for the observed $(H-K, J-H)$ depend little on whether the source is a dwarf or a giant (recall that the coincidence of the dwarf and the giant loci is what causes our actual problem) the relative distance is only determined by the difference in absolute magnitude meaning that if the star is a giant it is a factor ≈16 farther away than if it was a dwarf. Due to the ratio of the number densities the volume within the cloud distance based on the O – G6V stars will only suffer a slight contamination. Typically less than 5 contaminants are expected in front of a cloud at 150 pc and projected into one square degree on the sky. The volume beyond the cloud may contain a larger number of giants but here the extinction may work in our favour. For a cloud at a distance ≈200 pc the giants may sample a volume out to about 2.5 kpc meaning that they may pick up an additional extinction of A_V = 2 – 3 mag from the diffuse medium alone. This additional extinction will may push them beyond the upper extinction limit of A_V ≈3 mag pertinent to the zone between the upper reddening vector and the main sequence locus so we are pretty confident that most of the K dwarf candidates are real dwarfs.

An example of the resulting $(1/\pi_{JHK},\ A_V)$ distribution from the three groups of tracers is shown in Fig. 39 for the 2×2 □° area centered on $(\alpha,\ \delta)_{center}$ = $(18^h24^m,\ 0°0')$ adjacent to clouds A and B, Harvey et al. ([2007]) in the star forming Serpens cloud. The color – color diagram for 2×2 □° is the black underlying points in Fig. 37. We note that the extinctions are different in these three Serpens regions. The regions containg the A

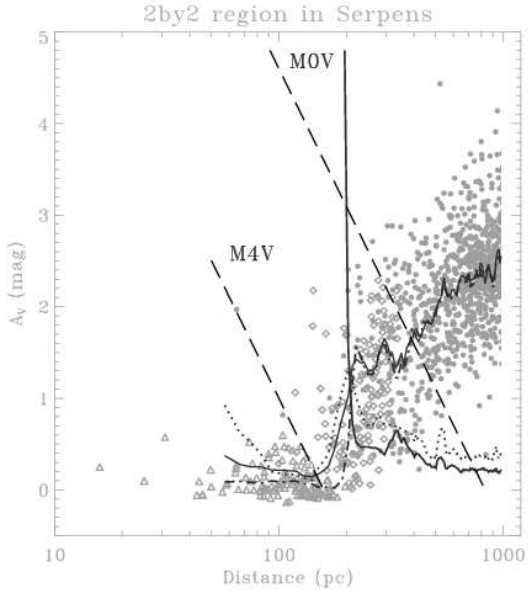

Figure 39: Distance vs. extinction diagram for the 2×2 □° region centered on part of the star forming Serpens cloud with $(\alpha,\ \delta)_{center,2000}$ = (18^h24^m, 0°0′). The two-color diagram for these stars region may be seen in Fig. 37. Triangles are the $M4 - T$ dwarfs, diamonds the proposed G6 – K9/M0 dwarfs and finally the larger black filled circles are the dwarfs earlier than G6. The distance axis is shown on a logarithmic scale in order to emphasize the closest stars. The two dashed lines display the maximum extinction observable with a $M4V$ and a $M0V$ tracer respectively with J_{lim} = 14.5 mag. The statistics are sampled in 20 pc distance bins with distance steps of 10 pc. Each distance bin has a 50% distance overlap with each of its adjacent bins. The solid curve displays the run of the mean extinction $< A_V >$, the dashed curve is the variation of the median extinction. The dotted curve is the standard deviation/sqrt(N-1) scaled with a factor five for clarity. Finally $\sigma_{A_V}/\overline{A_V}$ is shown as the solid curve in black. The statistics for this curve are clipped below 100 pc where it shows some oscillations

and B clouds are generally more obscured than the 2×2 □° area.